THE TIME OF FLIGHT METHOD APPLIED TO 2.37 MeV NEUTRONS

by

Tung-Hong Hsu

Submitted in partial fulfilment
of the requirements for the
degree of Master of Science.

Department of Physics
Faculty of Pure and Applied Science
The University of Ottawa
Ottawa, Canada.

1964

Approved for the
Department of Physics

Supervisor

Chairman of Examining Committee

Chairman of the Department

ABSTRACT

A time of flight system using an associated particle detector was developed for use with DD neutrons of 2.37 MeV. As part of this system a new method of neutron gamma discrimination based on the Owen principle was developed; this method distinguishes 0.5 MeV neutrons from a very wide energy range of gamma rays. This apparatus was then used to measure the angular distributions of the neutrons scattered from the ground state and the 0.845 MeV state of Fe^{56}.

ACKNOWLEDGMENTS

The author is indebted to his supervisor Professor J. M. Robson for suggesting the problem and for his generous encouragement. He would like to thank Mr. W. J. Mc Donald for the generous loan of his transisterized time-to-amplitude converter and for many helpful discussions. He is also grateful to his colleague Mr. D. Gedcke for many useful discussions. Thanks are also extended to Mr. G. Cornish for maintenance of the accelerator and many helpful technical suggestions, Mr. Goodchild, for construction of target assembly, Mr. R. Hart for construction of neutron detector shielding, and Mr. C. Spira for helpful comments on the manuscript.

TABLE OF CONTENTS

LIST OF ILLUSTRATIONS

CHAPTER I

INTRODUCTION

Much attention has been paid to the inelastic and elastic scattering of neutrons by nuclei, at energies around 14 MeV, where direct interaction and the optical model become important. This is primarily because neutrons of this energy can easily be produced in large numbers by means of the $T(d, n)He^4$ reaction. It is also because neutrons in this energy range can easily be detected by several methods such as (i) the emulsion technique[1], (ii) the shell transmission method[2], (iii) the cloud chamber method[3], and (iv) the time of flight method[4)-9].

However, neutron scattering data are very scarce in the energy region of a few Mev[10)-13], where compound nucleus reactions and the statistical model become important. It is more difficult to produce comparatively large numbers of neutrons in this energy range where one is restricted to the $Li^7(p, n)Be^7$ or $D(d, n)He^3$ reactions. Furthermore a neutron detection method incorporating good energy resolution and high efficiency is still difficult to achieve over most of this energy range, although it is now available for neutrons of energy below one Mev[20)-21]. Until now most of the scattering data of a few MeV neutrons have been restricted to the time of flight method using pulsed beam sources, to the emulsion technique[22)-23] or to the complementary use of neutron spectra and gamma ray measurements, together with coincidence techniques[24].

The pulsed source time of flight method, except that using terminal pulsed accelerators which are not yet widely available, has the disadvantage[25] of a high neutron background, a low neutron yield and great complexity.

Because of the difficulty in detecting the He^3 associated particles[26] from the D-D reaction, no successful work has so far been reported using the associated particle time-of-flight method in this energy region. It was the purpose of this work to develop this method for the study of the scattering of neutrons of a few MeV. Furthermore a new concept of neutron gamma discrimination based on Owen's pulse shape discrimination method[27]-[28] was developed and used in the present work in order to reduce the background. Preliminary measurements on the scattering from iron and aluminum were studied and the results are compared with work of other authors. Further improvements of the system and suggestions for possible measurements on some interesting nuclei, are given in later chapters.

CHAPTER 2

EXPERIMENTAL METHOD

2-1 Neutron Source

Neutrons of energy 2.37 MeV were obtained from the $D(d, n)He^3$ reaction. The unanalyzed deuterium ions were accelerated by a 125 kv electrostatic accelerator* and collimated to a beam of one eighth of an inch diameter. The beam was allowed to bombard a copper backed Zr-D target, containing 0.7 cc per square inch deuterium**. As shown in Fig. 1, the target sheet was attached at an angle of 30° with respect to the bombarding beam. In order to minimize the serious deposits which are always caused by low vapour pressure organic materials, such as diffusion pump oil, vacuum grease etc. on the target, no vacuum grease was used in the vacuum system. Instead, the target sheet was sealed to the target holder directly by a 1/16 inch indium wire gasket.

At ambient temperature of 20° C it was found very difficult to operate for more than half an hour, unless a forced cooling was employed, since the temperature rise of the target causes the D_2 to out-gas[29]. The target cooling was accomplished by spraying a fine jet of water directly onto the back side of the target.

Due to the low energy of the associated particles and the great difficulty encountered in their detection, the He^3 particles were detected at a lab. angle of 130°, instead of the customary 90° lab. angle. At this

---

* Texas Nuclear Co. 150-I.H. Neutron Generator

** Supplied by Texas Nuclear Co.

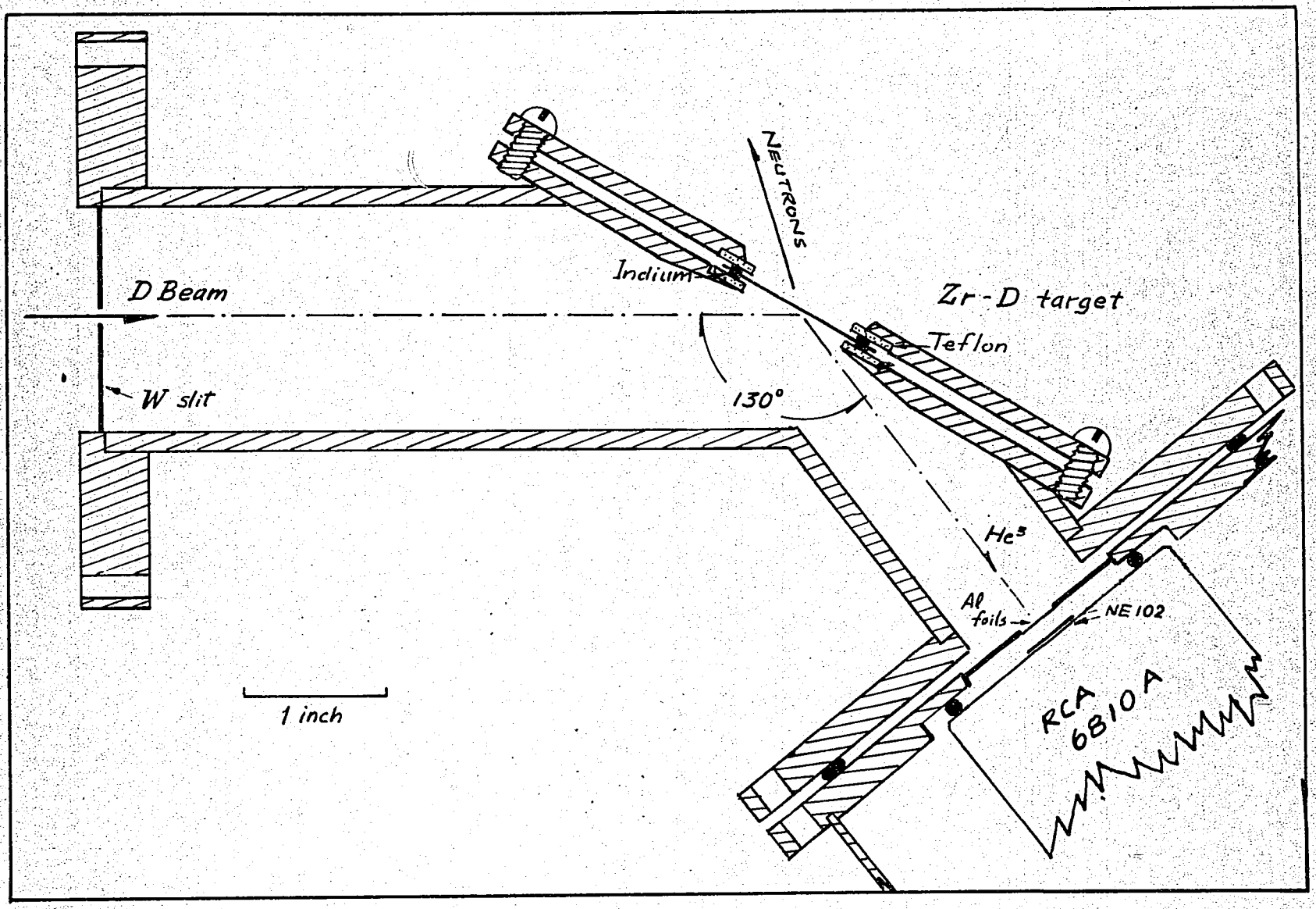

Fig. 1. Target assembly for D-D reaction and their associated particles detector.

angle, and at a bombarding energy of 120 Kev, the He^3 recoils had an energy 1.065 MeV compared to the 0.781 MeV which they would have had at 90°*.

The He^3 recoil particles were then collimated by a 1 cm x 2 cm rectangular aperture, located in the front face of the associated particle detector. This detector, a 0.0002 inch thick NE 102** plastic scintillator, subtending a solid angle of 0.031 sterad and located at an angle of 130° from the incident beam, detects charged particles with one hundred percent efficiency, and is located within the vacuum system. It was coupled directly to a RCA 6810A photomultiplier with Dow Corning DC 200 silicone oil. Two 150 microgram per square centimeter aluminum foils were placed on the collimator in front of the scintillator in order to block the direct and scattered deuterons as well as light from the target or ion source, and to improve the light collection from the scintillator.

Because of the very small thickness of this scintillator, the detection of the protons produced by the D(d, p)T reaction and of the gamma rays was minimized. Three RCA 6810A tubes and one CBS 1090 tube were studied, and among them the one with the best signal to noise ratio and comparatively fast rise time was selected for this purpose. The best operating conditions for this tube were found by making successive corrections to the first dynode, first grid, and anode voltages. With a 1/16 inch NE 102 scintillator an 18% energy resolution was obtained, from a partly collimated

---

* Appendix I.

** Supplied by Nuclear Enterprises, Winnipeg.

5.476 MeV Am^{241} alpha particle source.

Fig. 2 shows a typical spectrum for the charged particles from the D-D reaction. The high noise here, is mainly due to the detection of protons, and the broader peak to the pile up of He^3 and triton peaks.

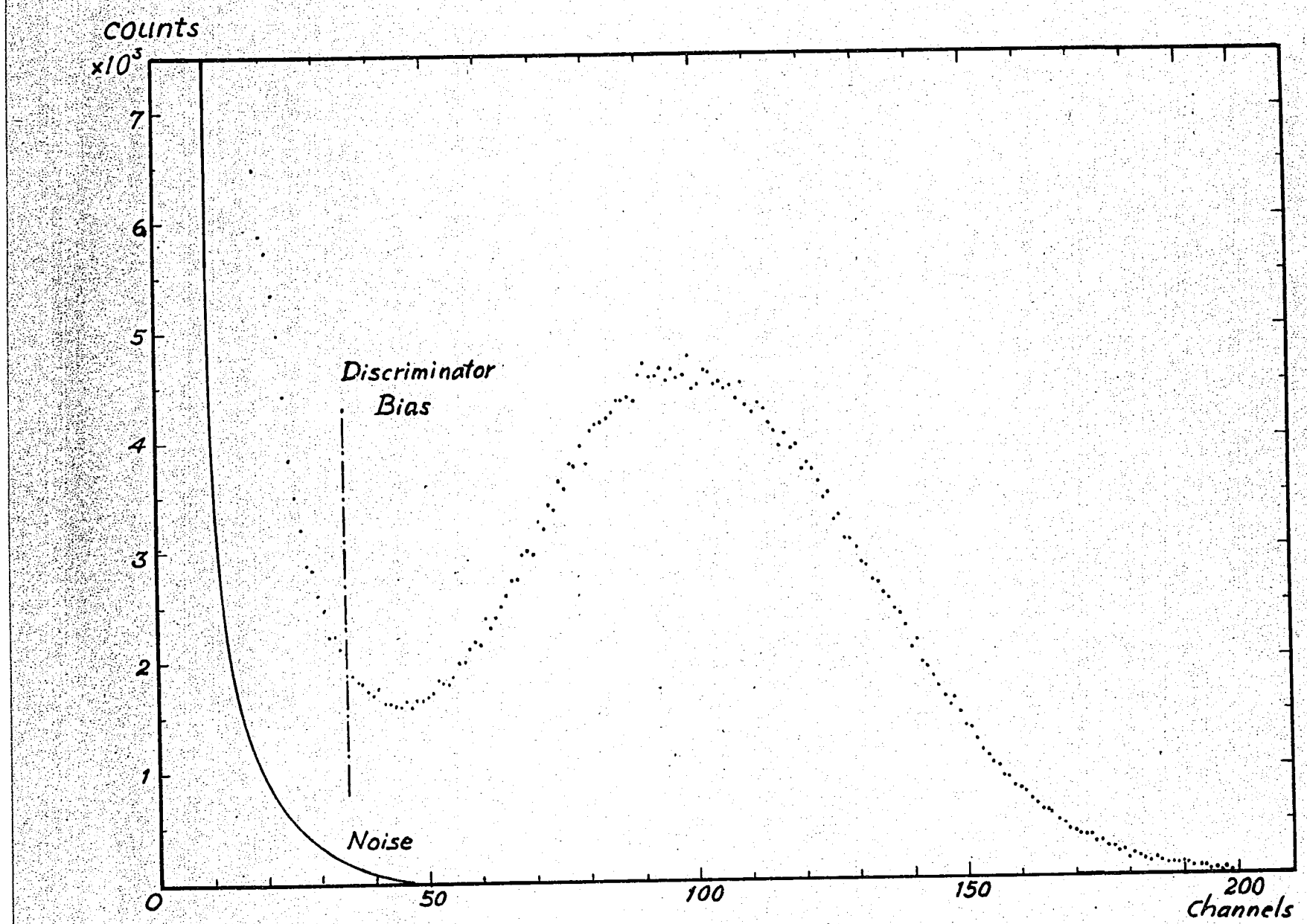

Fig. 2. Charged particle spectrum from D-D reaction.

2-2 NEUTRON DETECTOR

2-2-1 Neutron Gamma Discrimination

Two major advances in the technique of detecting neutrons with increased efficiency, reduced background, and faster time resolution have been reported: (i) the pulse-shape discrimination method and (ii) the glass scintillator method, in which the scintillator is loaded with enriched boron 10 or lithium 6.

The latter method, developed by Ginther and Schulman, and recently modified by C. Coceva[30], is more suitable for the detection of neutrons with energies less than one MeV, especially in the Kev region, because of the 1/v dependence of the (n, α) cross sections of boron 10 or lithium 6. For this reason, the former method is preferred for the detection of MeV neutrons. In 1956 Brooks first suggested and developed[31)-32)] circuitry capable of distinguishing fast neutrons from gamma rays by means of the different decay times of the recoil proton and electron scintillations. An improvement of Brooks' method has been reported by Daehnick and Sheer[33].

According to Firk[34], one of the disadvantages of this method is the long dead time, which can cause a serious problem where high background counting rates are encountered.

In 1958 R.B. Owen took another approach to this method by using the decay times of both the initial fast spike and the long-lived components. He achieved this by operating the last dynode of the photomultiplier in the saturation region[35]. If the potential difference between

the last dynode and the anode of the photomultiplier is made small, the space charge limitation of the anode current affects the linearity of the current gain at this dynode. If β is the secondary emission factor for the last dynode, which receives a current $-I_o$, the outgoing current from this dynode can vary from its normal non saturated value $-(\beta - 1)I_o$ to $-I_o$, depending both on the magnitude of I_o and on the dynode-anode voltage. Therefore, the voltages between the anode, grid no. 2 and dynode no. 14 can be adjusted, so that the large amplitude fast component of the signal produces a net negative current at the last dynode. After integration, the resultant voltage pulses can be negative for neutrons and positive for gamma rays.

Owen's method has been widely used in order to accomplish neutron-gamma-random noise discrimination[36)-37)]. However, the difference in the polarity of the pulses developed at the last dynode for recoil protons and for Compton electrons can only be obtained for a restricted region of pulse amplitudes with a given anode voltage setting.

Batchelor et al.[36)] examined the pulses obtained from the last dynode of the photomultiplier, wired in Owen's manner, and found it possible to take advantage of the different zero crossover times of neutron and gamma ray pulses, as shown in Fig. 3. It is possible to discriminate against higher energy gamma rays by making a delayed coincidence between these negative original pulses and their positive back swing pulses. Batchelor et al. achieved some good discrimination results by this method. This method, however, despite its complexity

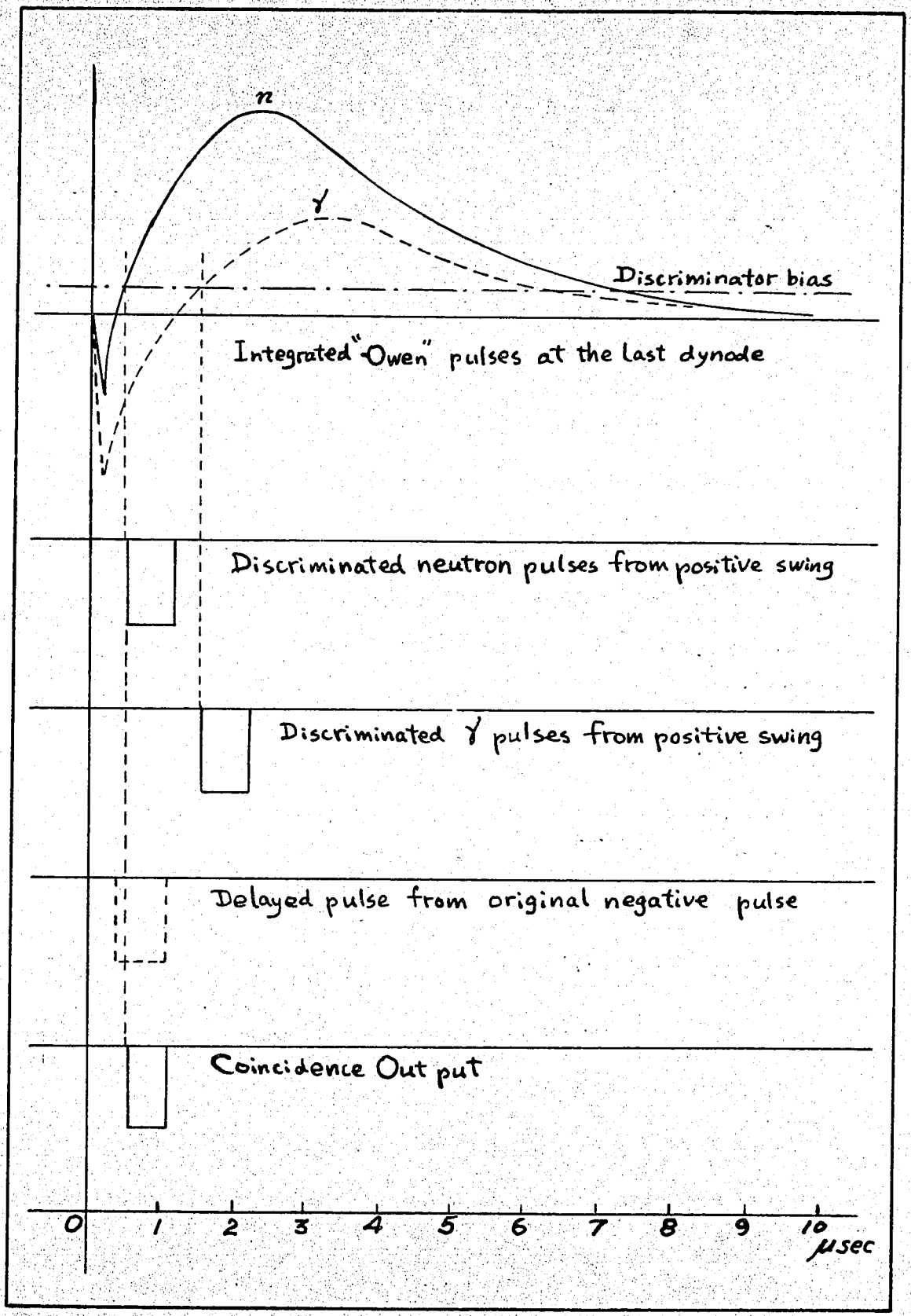

Fig. 3. Relative Owen pulses from 6 Mev gamma rays and 2 Mev neutrons, The pulse discrimination principle after Batchelor et al.

does not discriminate well against low energy gamma rays.

In the present work, instead of the delayed triple coincidence, the time-to-amplitude converter method[38] was applied to Owen's pulses. The saturation condition was first optimised using an oscilloscope two-parameter display as described in the block diagram in Fig. 4.

In Fig. 4 the integrated non distorted pulses from dynode 12 were connected to the y-plates of a Tektronix scope, through a plug-in Tektronix preamplifier (shown as Y-amplifier in the figure). The negative part of the integrated inverted Owen pulses (slow component) were amplified by a highly non-linear amplifier and applied to the x-plates of the scope. The positive part had very little effect on this amplifier. The positive parts of the integrated inverted Owen pulses were limited, passed through a time-to-amplitude converter which will be described later, a linear amplifier, and a single channel analyzer to the z-mode control of the Tektronix scope. This z-mode was made to modulate the intensity of the oscilloscope display on the screen, so that the scope would only trace events selected by the single channel analyzer. Sample oscilloscope photographs are shown in Plate 1.

Fig. 5 shows the circuit diagram of the preamplifier which incorporates the pulse shape discrimination. The 1N 904 fast diode is included to limit the huge negative swing of the last dynode integrated pulses, in order to reduce the blocking effects in the preamplifier. Then follows an inverter of gain two. The emitter follower in the slow output

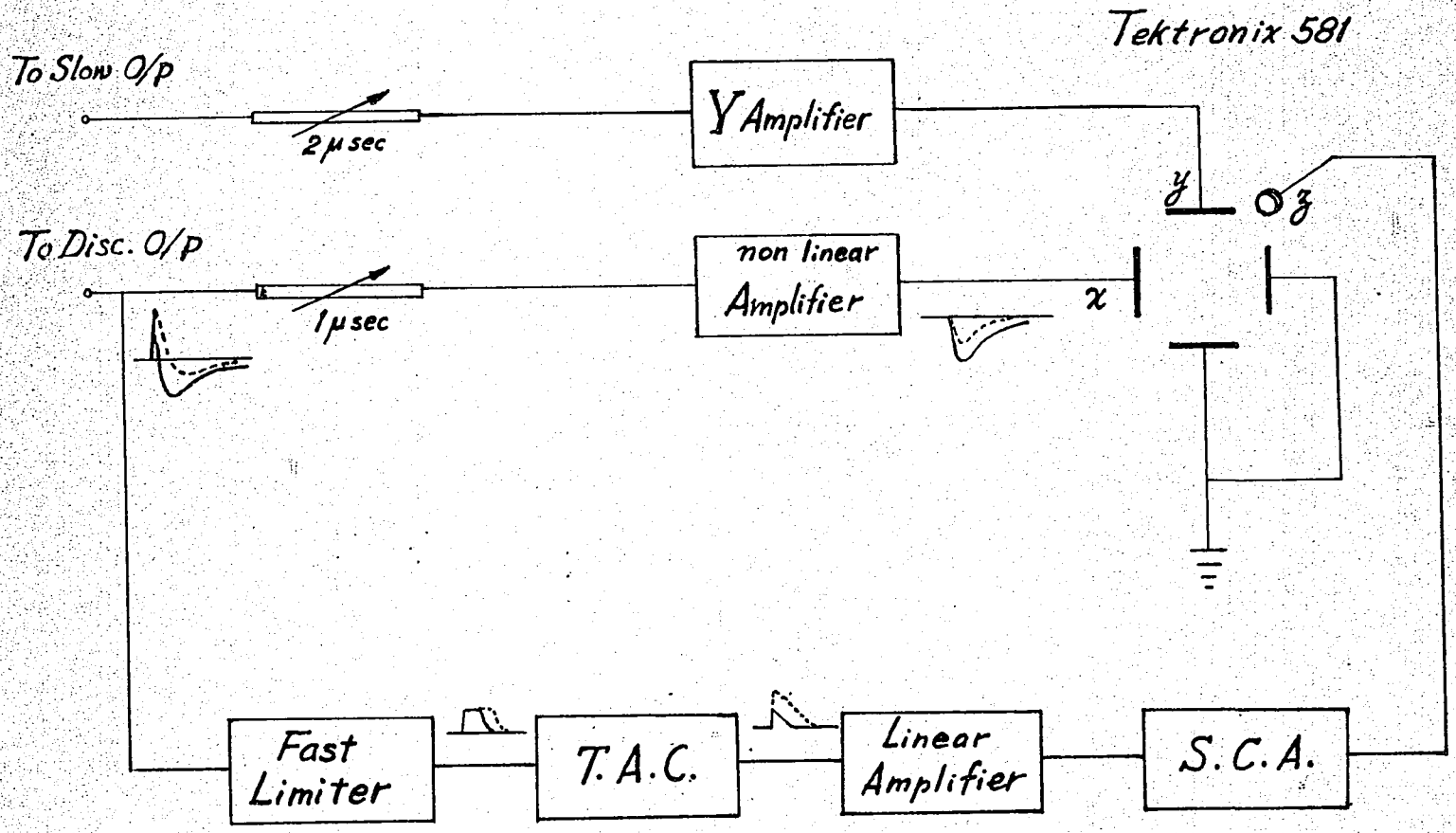

Fig. 4. Block diagram of electronic circuitry used for the oscilloscope two parameter display.

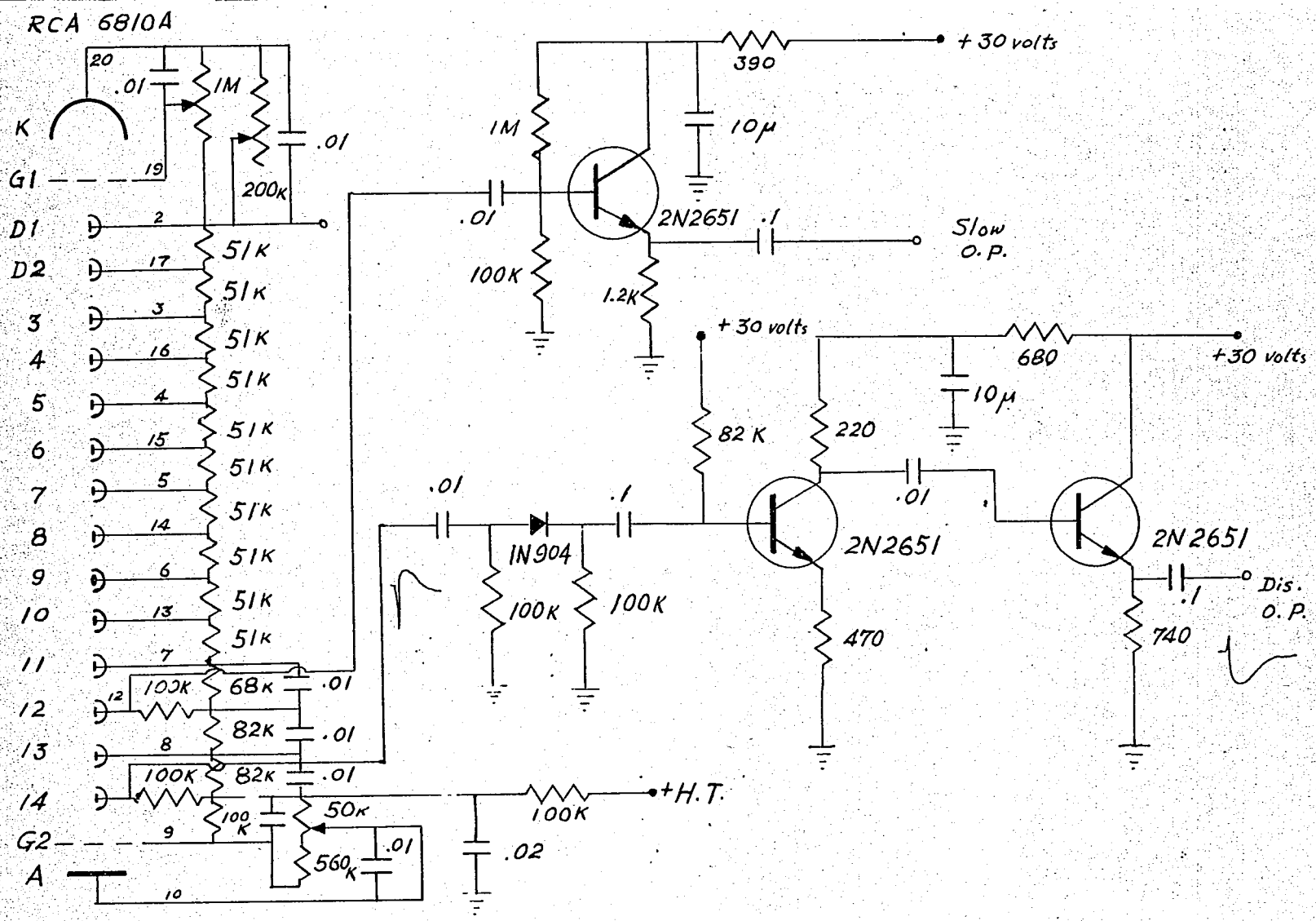

Fig. 5. Preamplifier with pulse shape discrimination for neurtron detector.

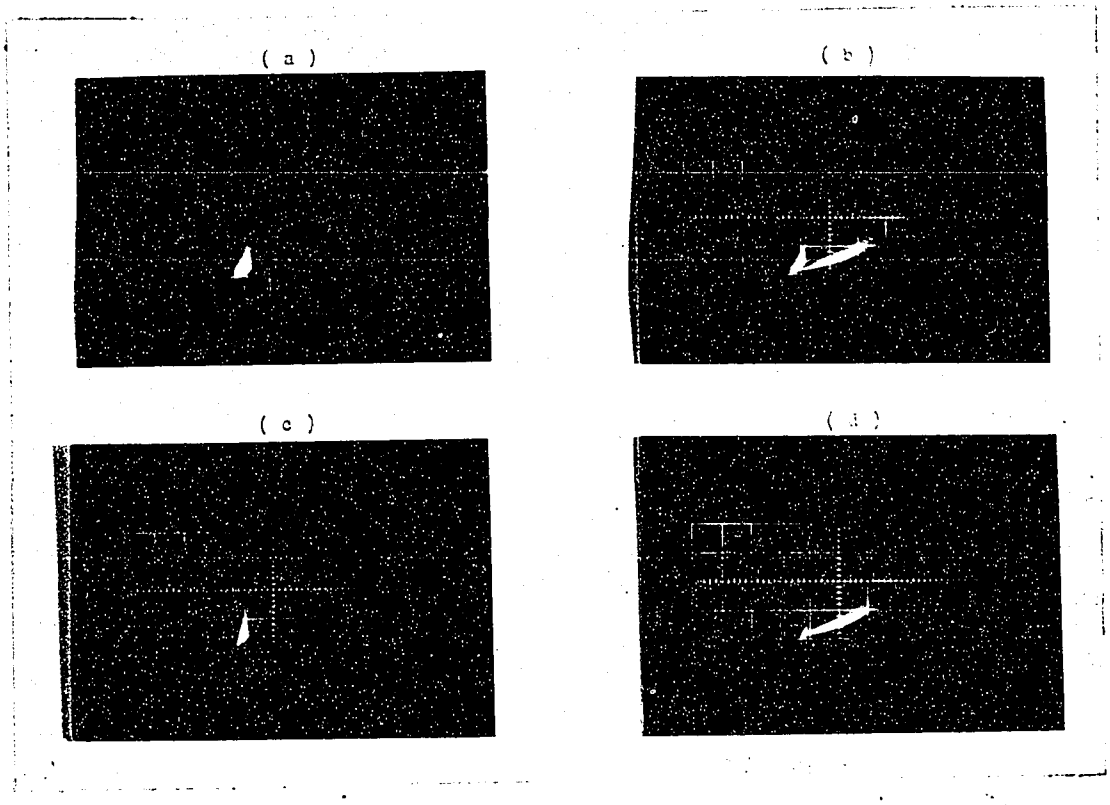

Plate 1 Oscilloscope 2 parameter display

(a) With Co^{60} and very strong Cs^{137} sources, without pulse discrimination.

(b) Ra-Be and Co^{60} sources, without discrimination.

(d) Ra-Be and Co^{60} sources, discrimination against gamma rays.

(c) Ra-Be and Co^{60} sources, discrimination against neutrons.

channel of the preamplifier is of conventional design. Following this preamplifier is a fast limiter similar to that shown in the upper part of Fig. 6. This limiter was originally designed by J.S. Fraser and R.B. Tomlinson of A.E.C.L., Chalk River. Only some constants were changed here for individual applications. Here, both transistors are 2N 1500, C_1 is 0.05 microfarad, and C_2 is 0.1 microfarad.

The positive part of the inverted pulses were limited to standard four volt positive pulses. They were then fed to a single tube 6BN6 Bell type time converter[39], shown in Fig. 7, by means of RG-65 cables. The purpose of this circuit is to subtract a constant time of 200 ns from all pulses so as to enhance the difference in the lengths of the pulses corresponding to neutrons and γ rays. Fig. 8 shows the pulse shapes and explains the principle of operation of the circuit shown in Fig. 7. The limited pulses were applied to the first input of the time converter and through a delay line of 200 nano-second length to the second input. Again, the cathode follower is of conventional design. Fig. 9 shows the spectra observed after this discriminator with (a) D-D neutron source, (b) Ra-Be source, (c) Cs^{137} gamma ray source. A window was determined, and the true events from neutrons were gated for slow coincidence which will be described in the next section.

The negative part of the inverted Owen pulses were amplified, discriminated, and put in coincidence with the pulses from the time to amplitude converter discriminator which was described in the last paragraph.

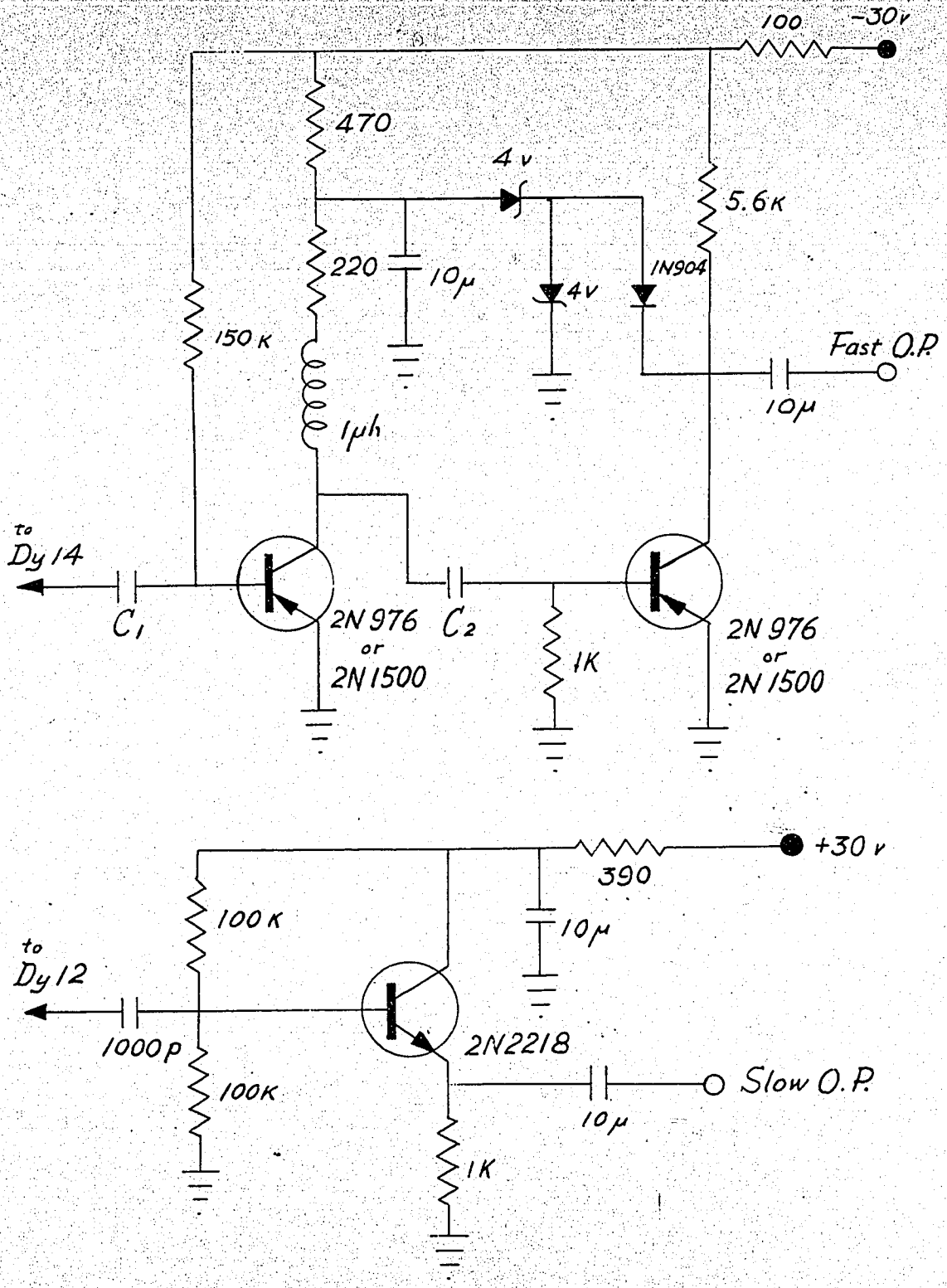

Fig. 6. Transistorized fast limiter and emitter follower.

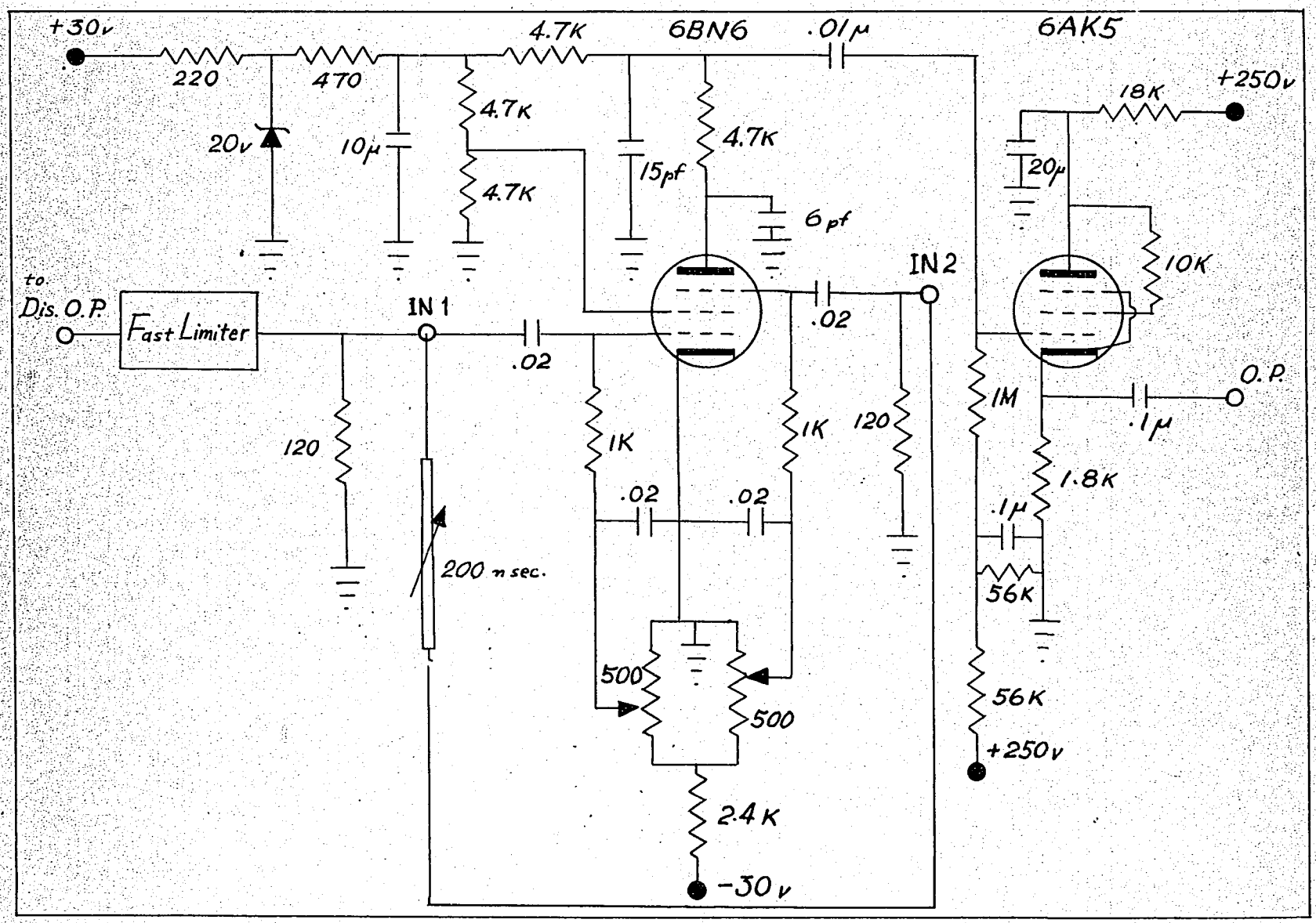

Fig. 7. Time-to-amplitude converter for neutron-gamma discrimination.

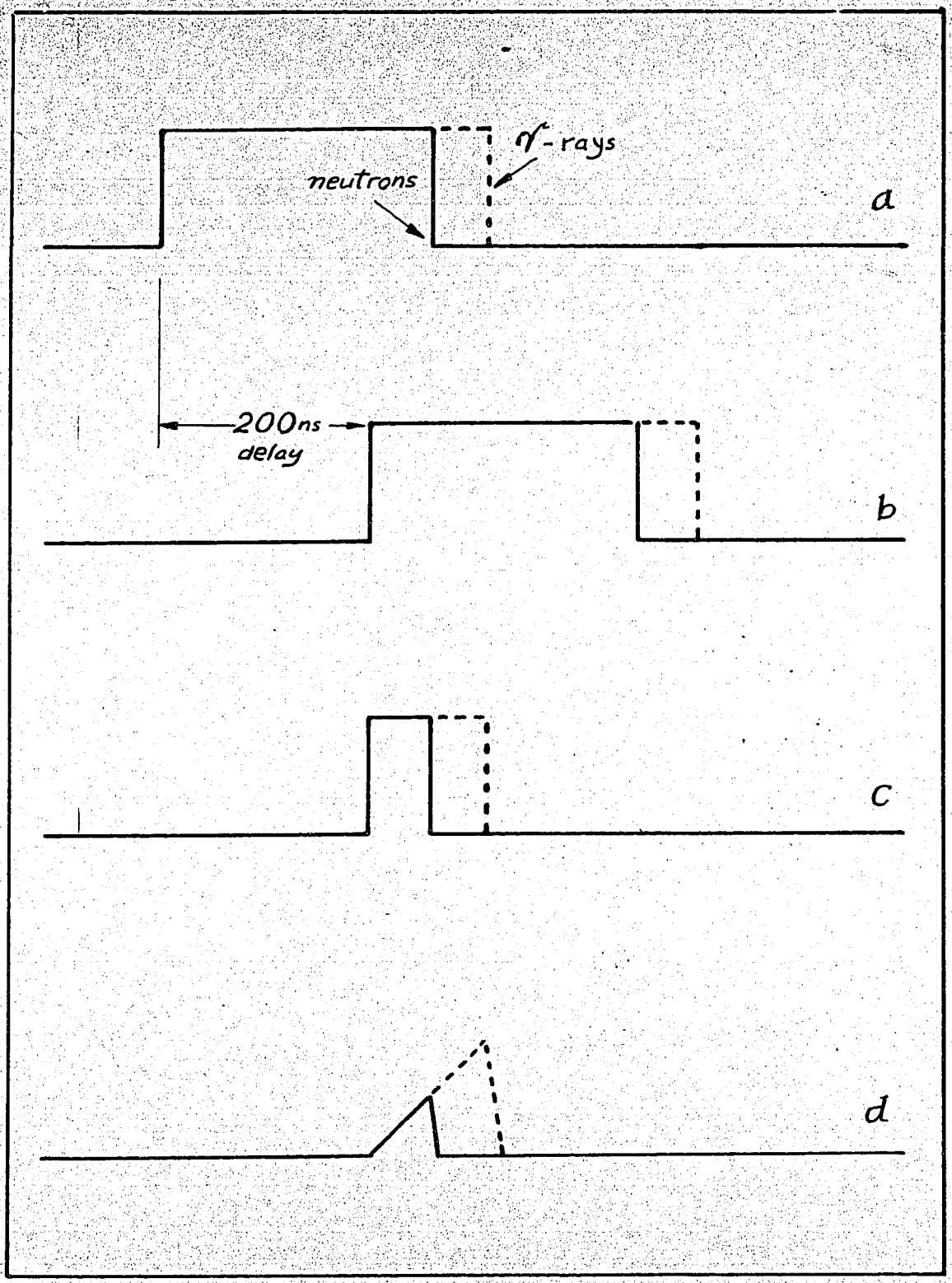

Fig. 8. Method of increasing the sensitivitv of the zero-crossing time measurement. (a) Signal at the first input of the time converter. (b) Signal at the second input of the time converter. (c) Plate current of 6BN6. (d) Resultant output of the time converter.

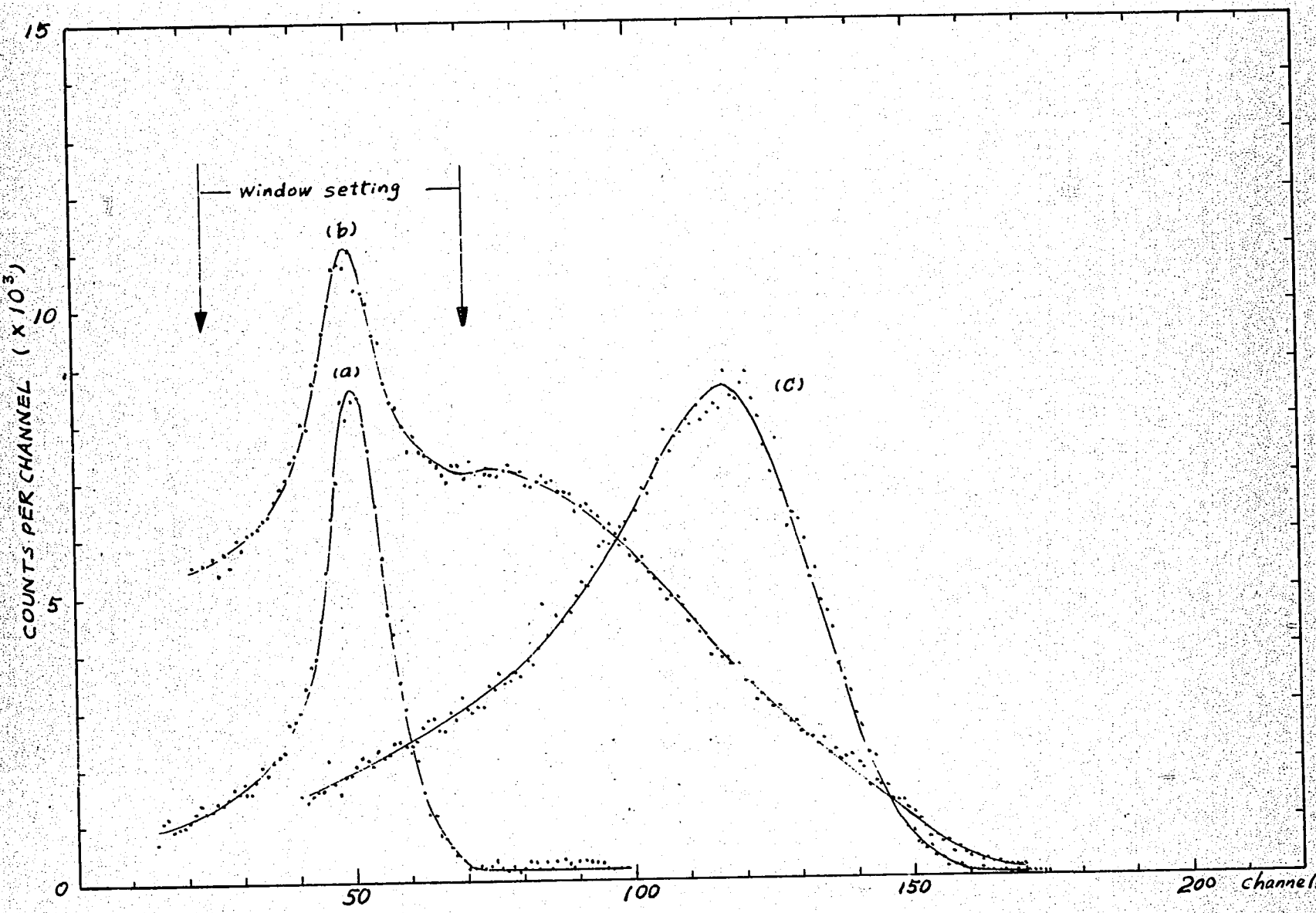

Fig. 9. Spectra of pulse shape discrimination from various sources. (a) D-D neutron source. (b) Ra-Be source. (c) Cs^{137} gamma ray source.

With the first discrimination one can separate the neutrons from high energy gamma rays, while the second discrimination avoids the detection of small energy gamma rays.

The neutron detector used was an organic liquid scintillator, type NE 213, supplied by Nuclear Enterprises, Winnipeg, contained in a horizontal type 2" x 2" glass cylinder which can be viewed from both ends. This scintillator was viewed by two RCA 6810A tubes as shown in the Appendix 4-4, Plate 2.

There are two signal outputs from both tubes. Fast signals from dynode 14 in tube A was coupled directly to a Fraser type fast limiter in which C_1 was 500 pf. and C_2 was 250 pf. A slow channel output was obtained by connecting an emitter follower to dynode 12 of tube A. The Owen pulses and another slow channel outputs were taken from tube B which was wired in the manner as shown in Fig. 6.

The effect of n-γ discrimination can be seen from Fig. 11. The time-of-flight spectra shown here were obtained from scattering of 2.37 MeV neutrons from Fe target at 90° laboratory angle. (b), (c) were obtained with pulse shape discrimination applied. Here inelastic and elastic peaks are well separated. These peaks are not separated in (a) where pulse discrimination was not applied and shielding was not adequate.

2-2-2 Detector Shielding

Shielding has been a serious problem in experiments which concern neutrons. There are two principal types of shielding: (i) complete shielding, and (ii) partial or shadow shielding. Although complete shielding has many advantages[40], it also has the disadvantage that the shielding materials are bulky and cause inconvenience of operation, especially for angular distribution or differential cross-section measurements. Only partial and shadow shielding was considered in the present work.

The main part of the present shield consists of a cylindrical tank of water, 58 cm in diameter and 100 cm height, as shown in Fig. 10. The detector was heavily shielded against gamma rays by constructing a cross-shaped tunnel from lead bricks. The inside dimensions of the tunnel were 5.5 cm x 5.5 cm, and the thickness of the tunnel wall was 5 cm. Further attenuation of the neutrons emitted directly from the source in the direction of the detector was obtained by piling up paraffin bricks in front of the main shielding tank. Additional shielding effect was achieved by placing a heavimet rod of 3 cm in diameter and 11 cm long in between the neutron source and the detector, where the shadow of the bar will completely cast on the neutron detector. By placing this shadow bar, the signal to noise ratio was boosted from 4.8 to 10 for the elastic peak from Iron target at 90° as shown in Fig. 11. Fig. 11(a) is the time-of-flight

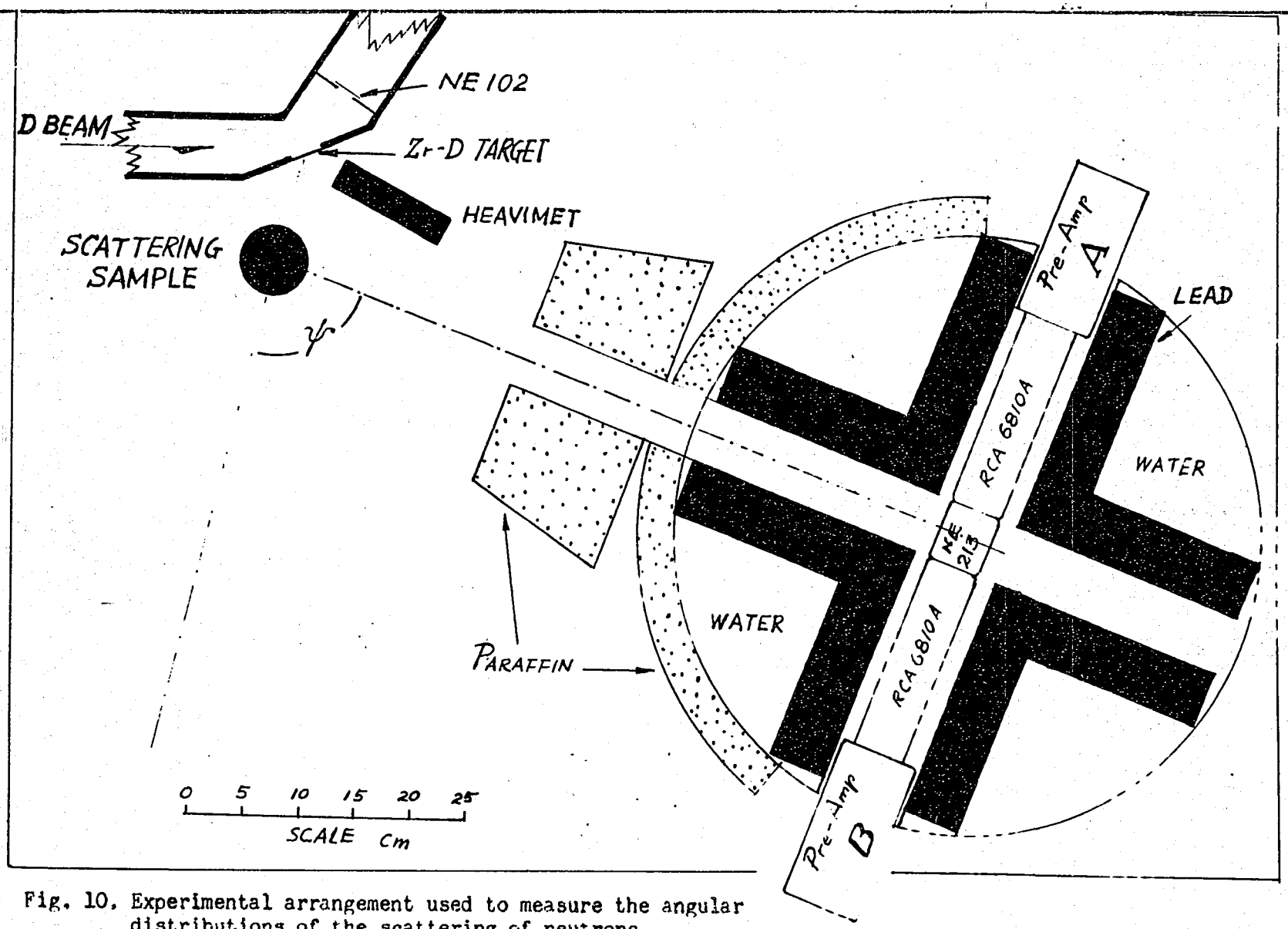

Fig. 10. Experimental arrangement used to measure the angular distributions of the scattering of neutrons.

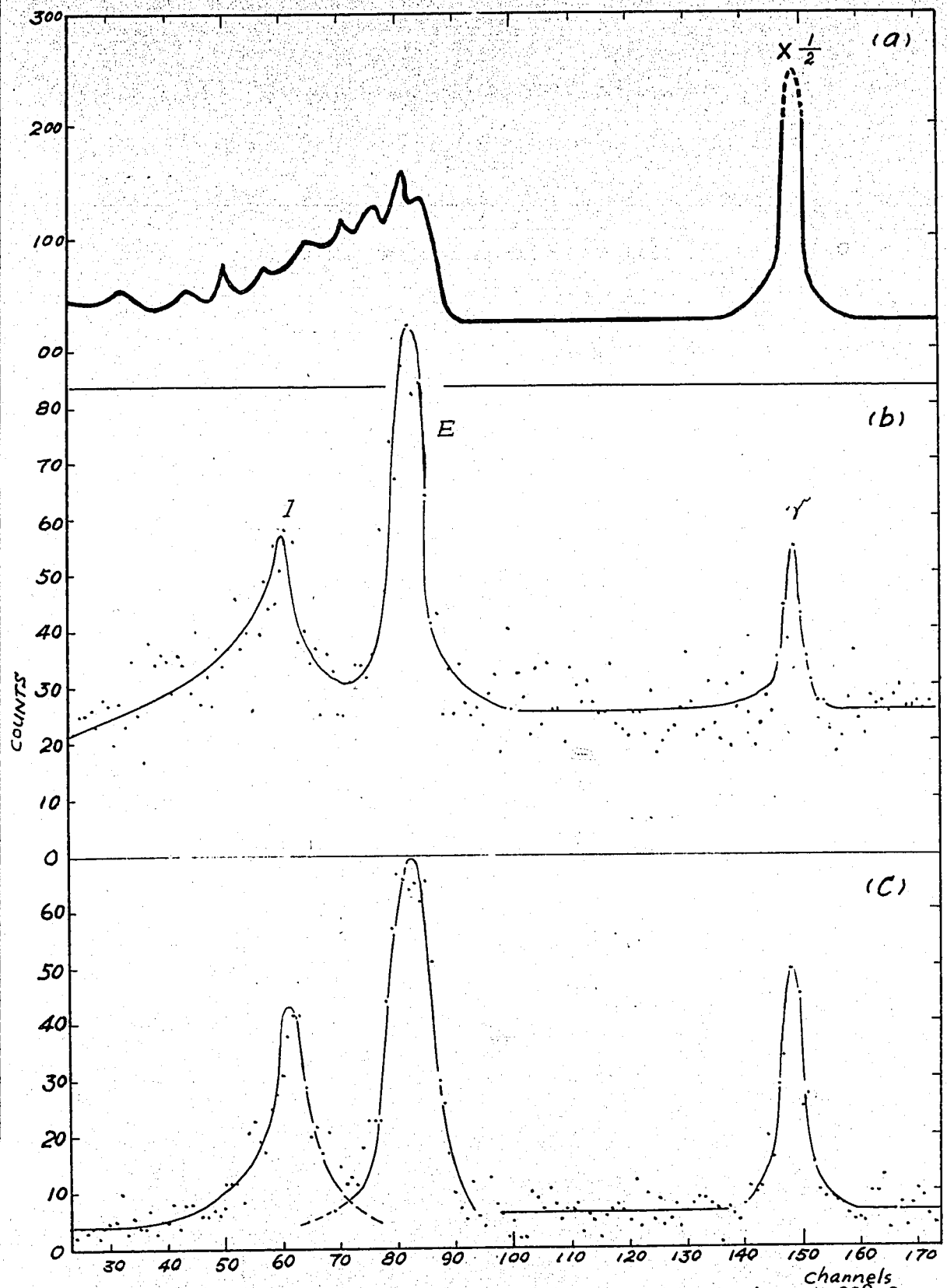

Fig. 11. The time-of-flight spectra of the neutron scattering at 90° from an iron scatterer. (a) without neutron-gamma discrimination. (b) with neutron-gamma discrimination but without shadow bar. (c) with neutron-gamma discrimination and shadow bar.

spectrum for the neutron scattering from iron scatterer at 90° without the heavimet shadow bar; (b) is the spectrum obtained at the same conditions as that of (a) but with the heavimet shadow bar. A side view of the detector shielding can be seen in Appendix 3, plate 2.

2-3 The Time of Flight System

The basic principle of the neutron time-of-flight system has been reviewed by many authors[41)-42)]. Only details particular to the present work will be given here.

In the present system, a cylindrical scatterer was placed 15 cm apart from the Zr-D target at an angle of 60° 15' with respect to the direction of the bombarding deuterium beam. The neutron detector was set at an angle ψ with respect to the direction of the impinging neutron beam, at distance of one meter from the centre of the scatterer. With the present shielding system ψ could be changed from 20° to 180° continuously.

Fig. 12 shows the block diagram of the time-of-flight electronic system including the pulse shape discriminator which has been described in the last section. Here slow channel outputs from both sides of the neutron detector were biased by the fast discriminator and then put into triple coincidence with the slow pulses from the He^3 detector as shown in Fig. 13. This reduced random coincidences, enabling the neutron detector to be biased well into the noise, so that low energy neutrons would be detected. Following the triple coincidence-I was the same fast discriminator which would produce a standard pulse of 5 nano-seconds rise time, 2 volts pulse height and 0.2 micro-seconds in width. These pulses were applied to open (prime) the gate of the time-to-amplitude converter*. Fast pulses from the photomultiplier tube A

---

* Courtesy of Mr. John MacDonald

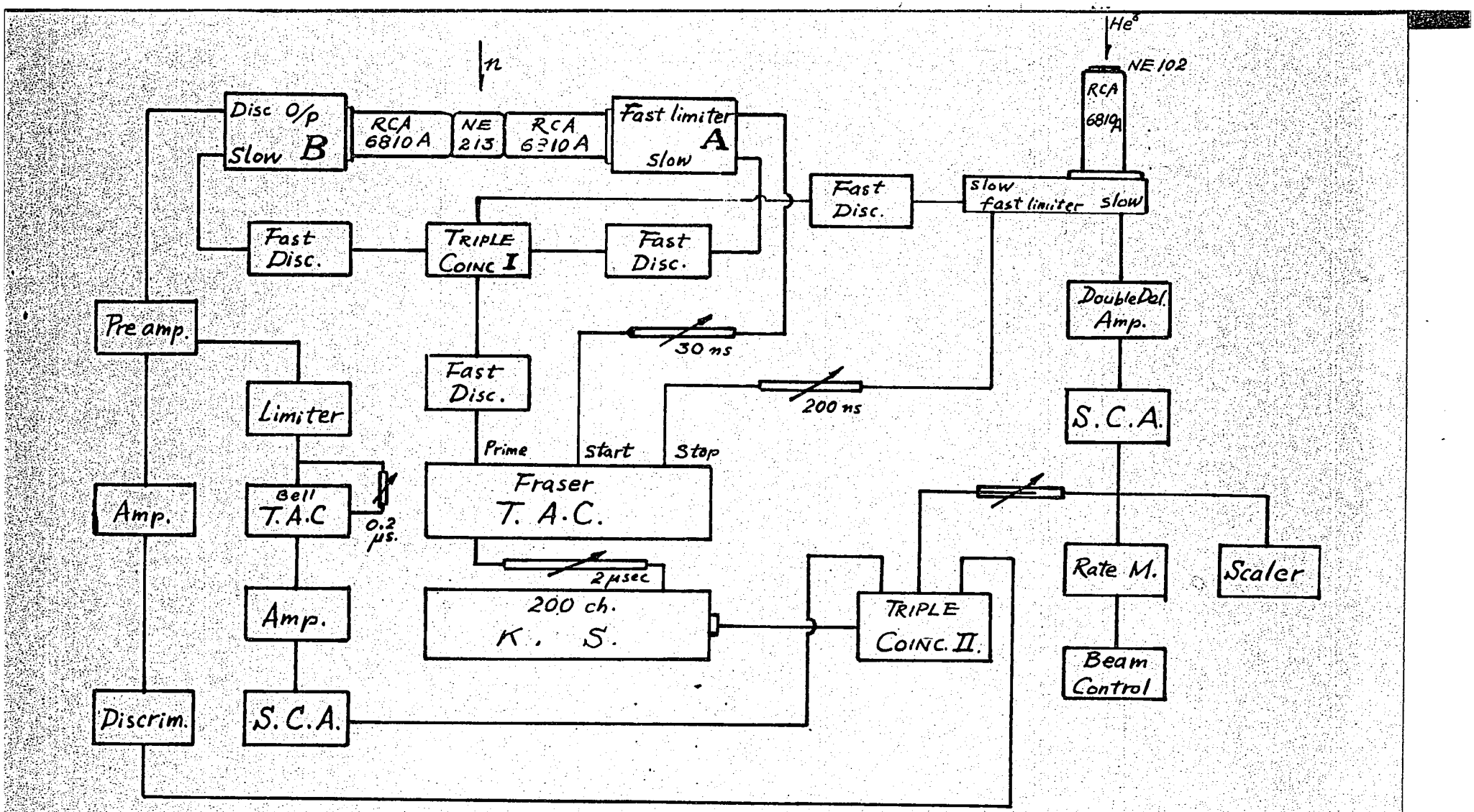

Fig. 12. Block diagram of the electronic circuitry used in the time-of flight system.

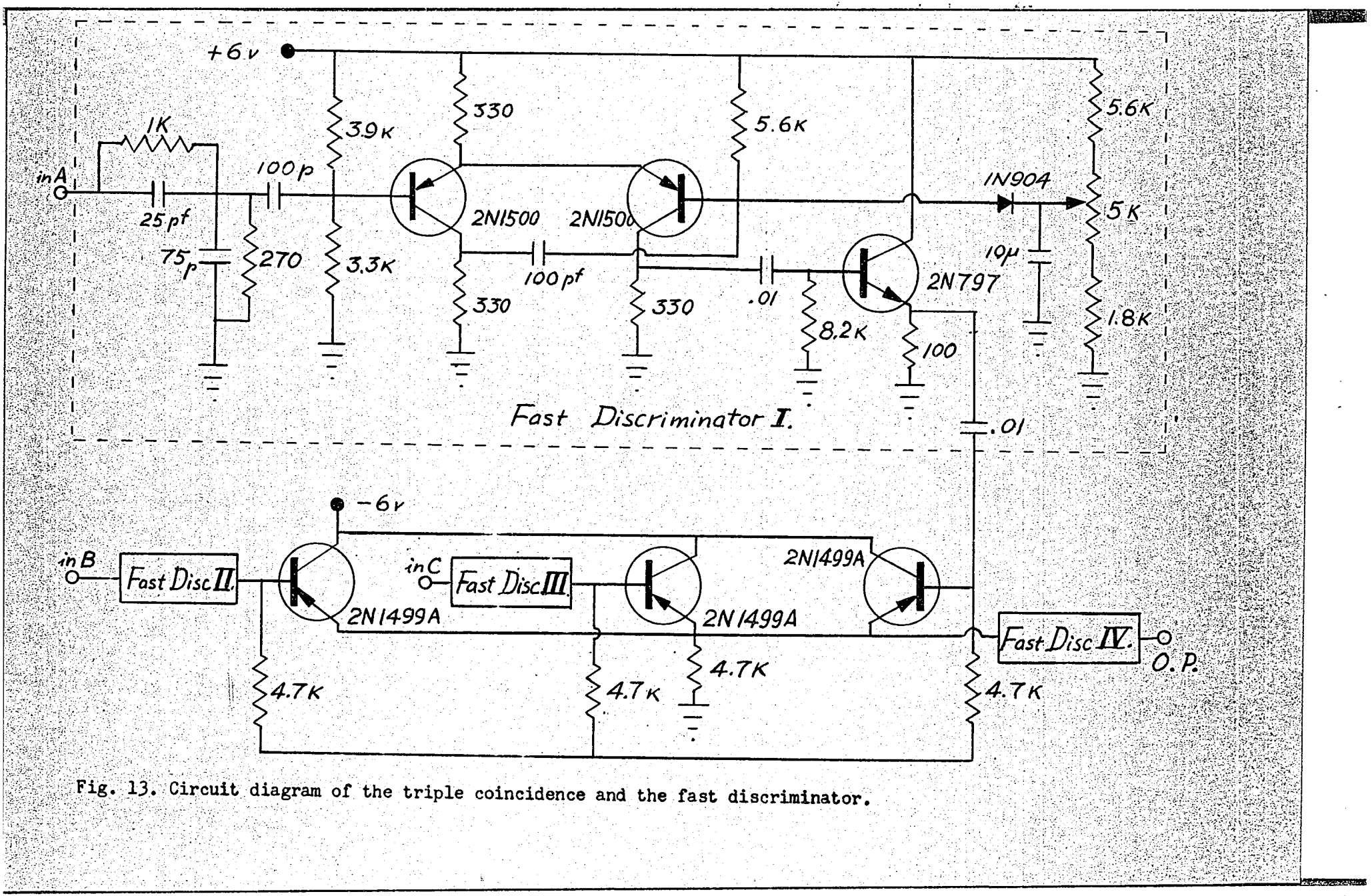

Fig. 13. Circuit diagram of the triple coincidence and the fast discriminator.

were limited to 4 volts positive pulses and were delayed 30 nano-seconds to the time-to-amplitude converter as the start pulses. The stop pulses were obtained from 0.2 micro-seconds delayed 4 volts limited pulses after the fast channel output of He^3 detector. Relationships between pulses and their delay times can be seen from Fig. 14.

The output of the time-to-amplitude converter was fed to a 200 channel Tullamore ST 200D analyzer which was gated by a slow triple coincidence II, the coincidences from Owen discriminated pulses, their selected discriminated pulses (see section 2-2-1) and slow He^3 pulses.

The He^3 detector also detected H^3 particles which were produced by $d(D, H^3)p$ reaction. Therefore, counting from this detector showed only relative numbers of outgoing neutrons. The method of the absolute counting will be given in the next chapter.

The angle of the neutron beam was determined by measuring the angular distribution of the neutrons from the neutron source directly. Fig. 15 is the neutron intensity distribution curve obtained this way. The angular spread was about 6.5 degrees in the present system.

Fig. 16 is a typical spectrum from the direct beam of D-D neutrons. The time resolution, FWHM (the full width at half maximum) for 2.37 MeV neutrons at flight path of 77 cm was 3.8 nano-seconds. The transit time in the scintillator was estimated as 2.4 nano-seconds.

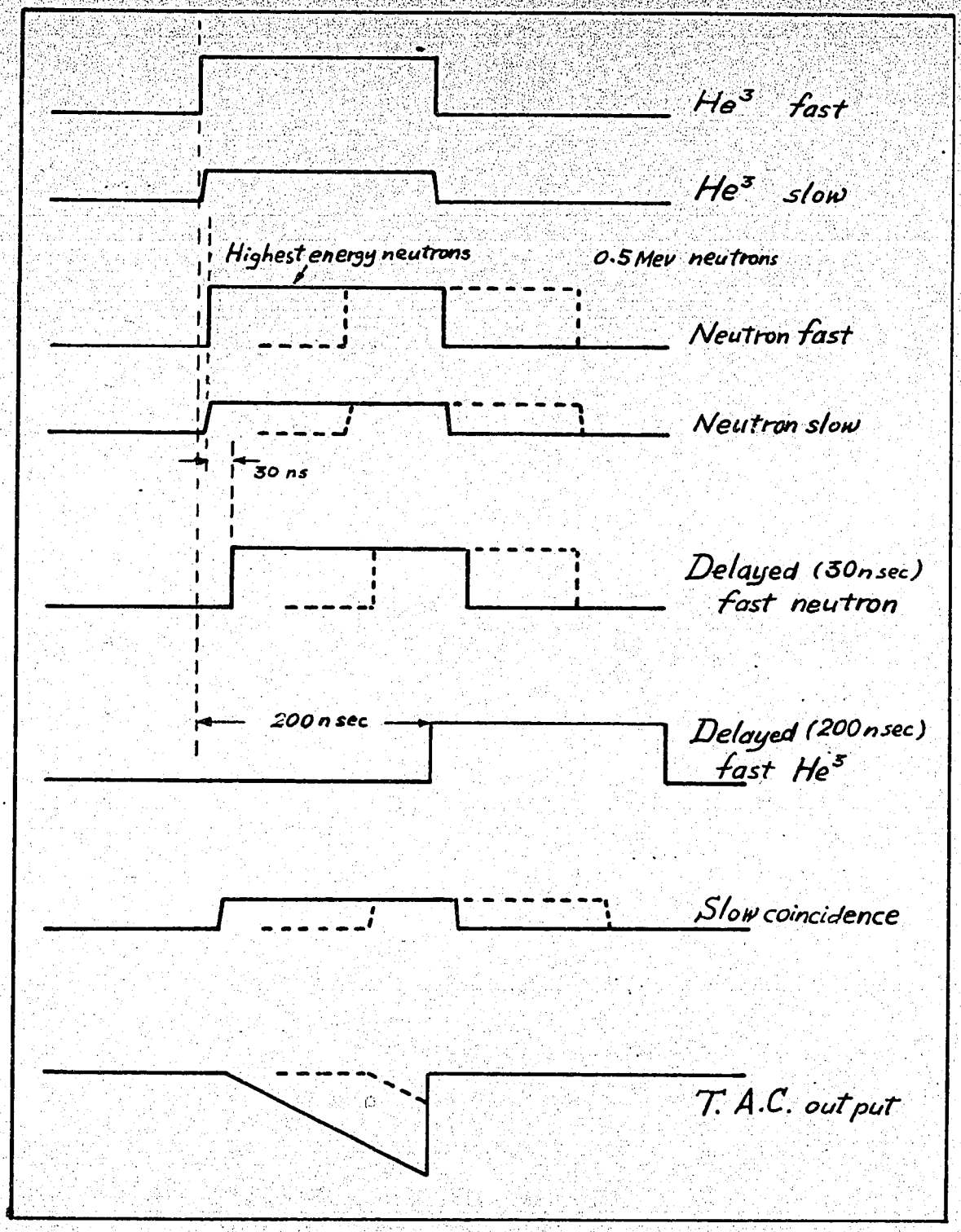

Fig. 14. Pulse chronology and duration.

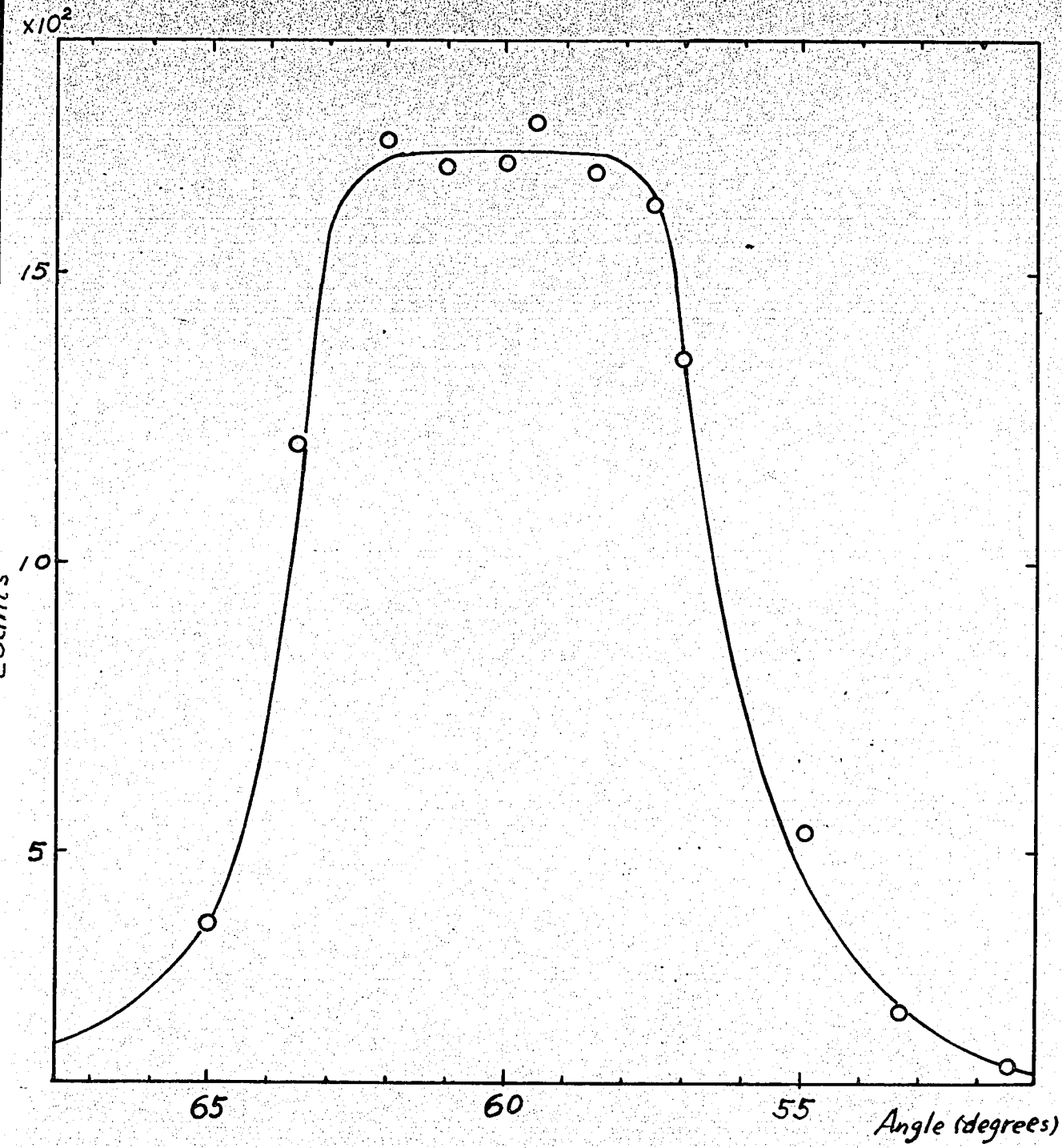

Fig. 15. The neutron beam distribution.

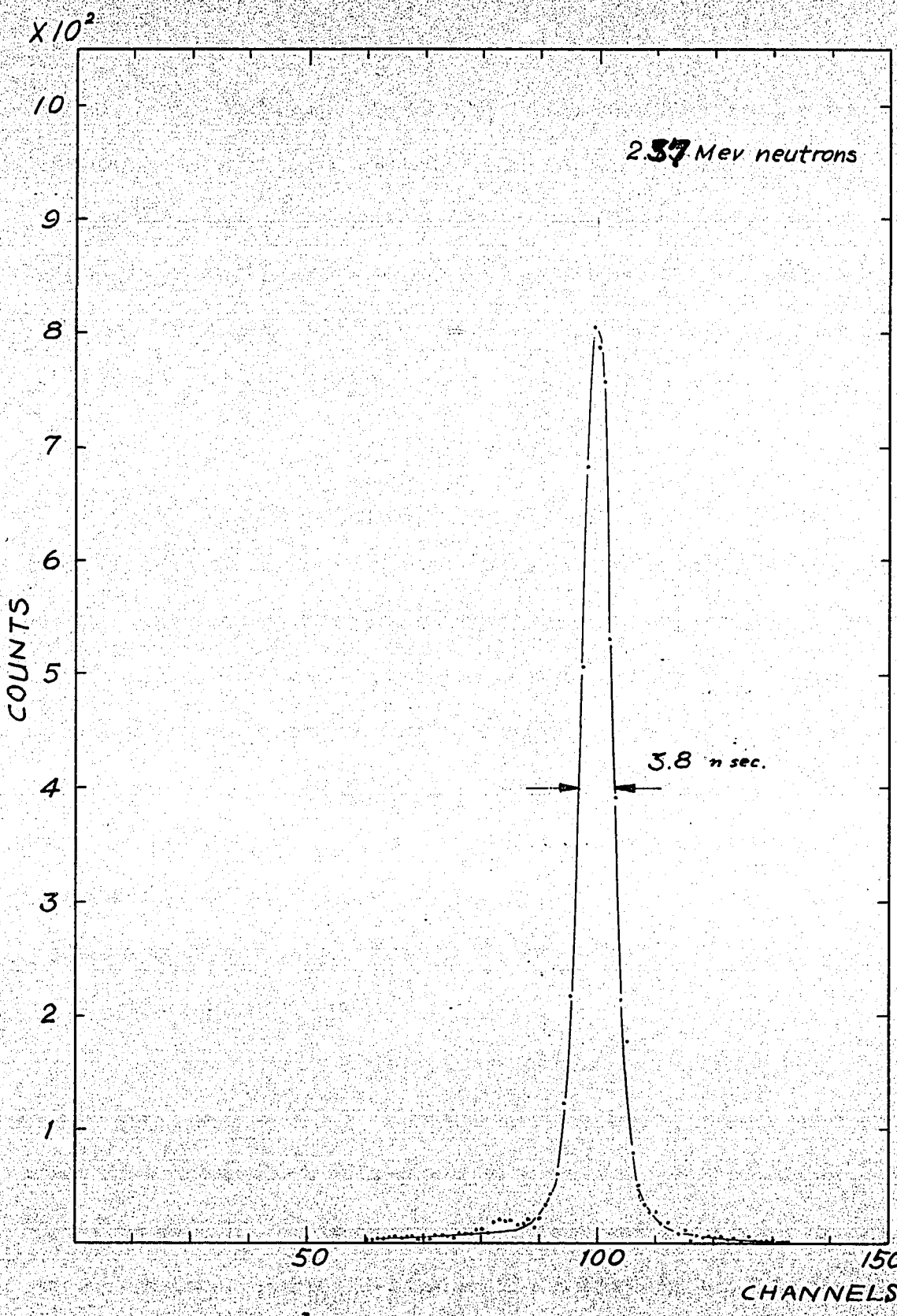

Fig. 16. The typical spectrum from the direct beam of D-D neutrons.

The spectrometer efficiency is defined as the product of the detector efficiency by the solid angle that it subtends. Experimentally the efficiency of the neutron counter was determined by detecting neutrons scattered by a rectangular polyethylene plate of 5 cm x 5 cm x 0.5 cm. The relative efficiency curve is shown in Fig. 17. This curve is in agreement with the shape calculated from

$$\varepsilon(E) = n\, h\, \sigma \left(1 - \frac{B}{E}\right)$$

where n is the number of hydrogen atoms in 1 cm^3 of the neutron scintillator; h is the thickness of the scintillator; B is the threshold of the neutron detector. In the present system we were interested only in the MeV neutrons, considering the linearity of the time-to-amplitude converter, pulse durations in the system were arranged in the manner of Fig. 14, so that the time-of-flight spectrum will cover the range approximately from 0.5 MeV neutron to gamma ray produced from the scatterer. Therefore the detection threshold was determined by the time delay of the fast neutron pulses and their durations rather than the direct bias set in the neutron counter itself.

The linearity of the time-to-amplitude converter was tested by changing length of RG-64/U cables as delay line. The linearity of the whole system was checked frequently between runs, by measuring the flight time of 2.37 MeV neutrons directly from neutron source to the neutron detector. In Fig. 18 straight line A was obtained from the neutron flight measurements, and B was obtained from delay line measurements.

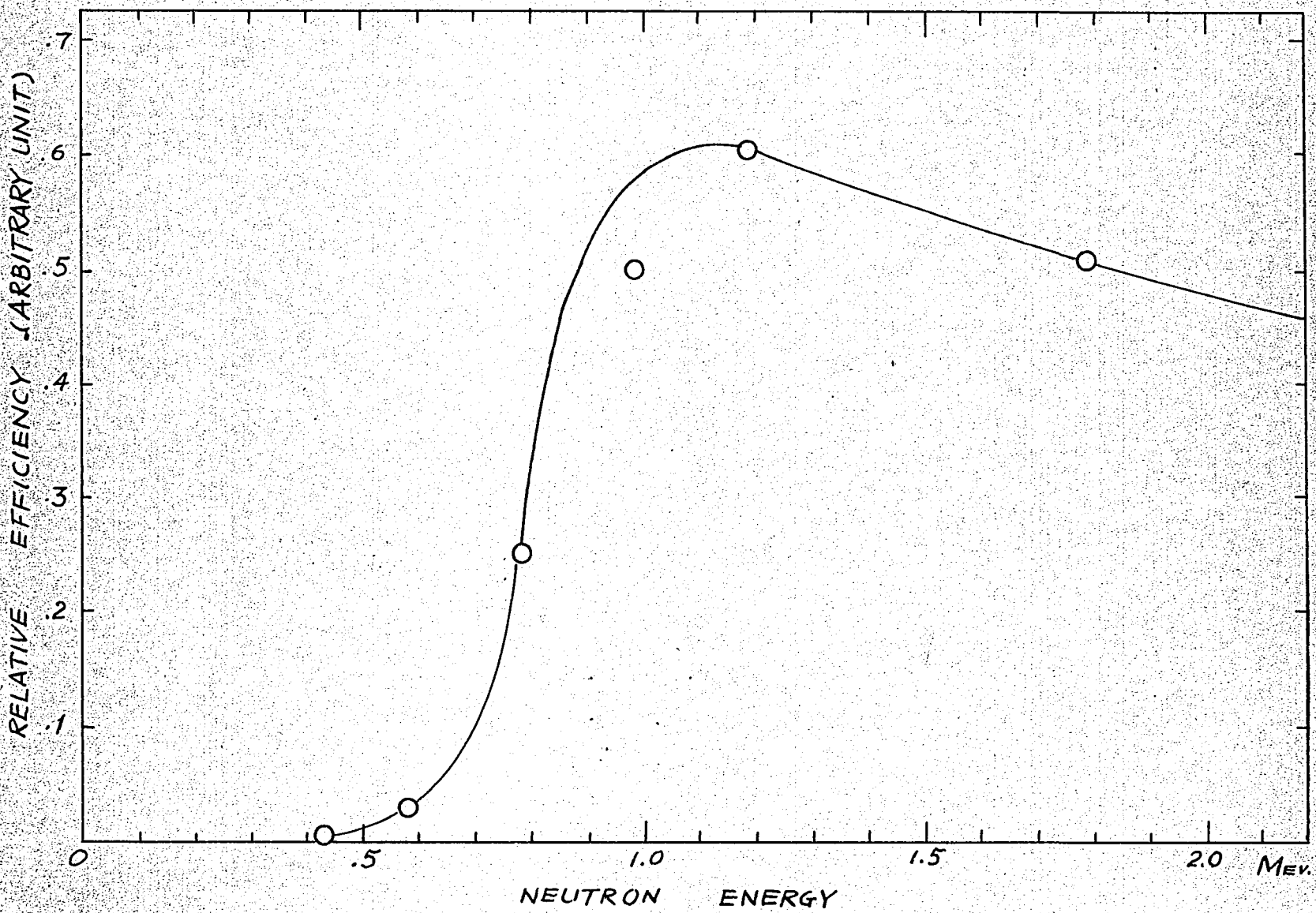

Fig. 17. The neutron counter efficiency curve.

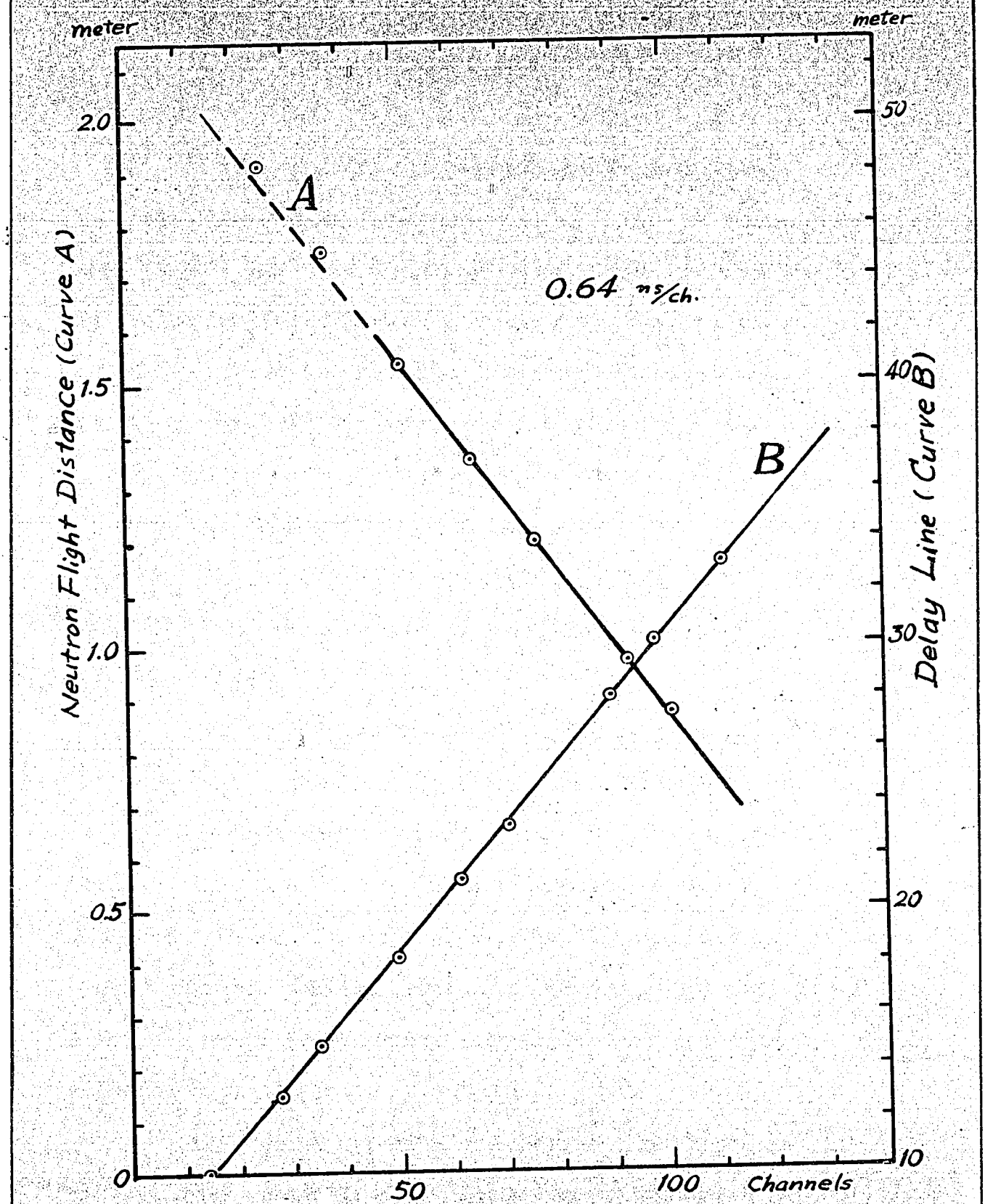

Fig. 18. The T.A.C. linearity and its time interval per channel determination.

CHAPTER 3

RESULTS

A mild steel rod of 11.5 cm height, 5 cm in diameter was put at the position of the "scatterer sample" in Fig. 10. The neutron flight distance was 95 cm measured from the scatterer to neutron detector and the distance between the neutron source and the scatterer was 6.5 cm. It took 20 hours to accumulate the counts shown in Fig. 11 at a scattering angle of 90° in the laboratory system. The peak in the spectrum marked as "γ" is due to the direct gamma rays produced in the scatterer. The peaks "E", "I", correspond to elastic scattering and to inelastic scattering from the 0.845 MeV level in Fe^{56}. The energy of the first level was measured using the elastic peak and γ peak as reference points.

The angular distributions for elastic scattering and inelastic scattering to the 0.845 MeV level obtained at 2.37 MeV incident neutrons were then measured and are shown together with the results from L. Cranberg and J.S. Lewis[11], and those of Landon et al.[13] in Fig. 20. Cranberg's elastic scattering data were obtained with 2.25 MeV neutrons while the inelastic scattering data are an average of data taken at 2.25 and 2.45 MeV; with 2.2 MeV incident neutrons for both the elastic and inelastic scattering in the case of Landon's work.

The results, presented in the centre of mass system[43] have not been corrected for absorption and multiple scattering in the solid target, though some serious effect had been observed at backward angles with the present target. The measurements were performed alternately with and

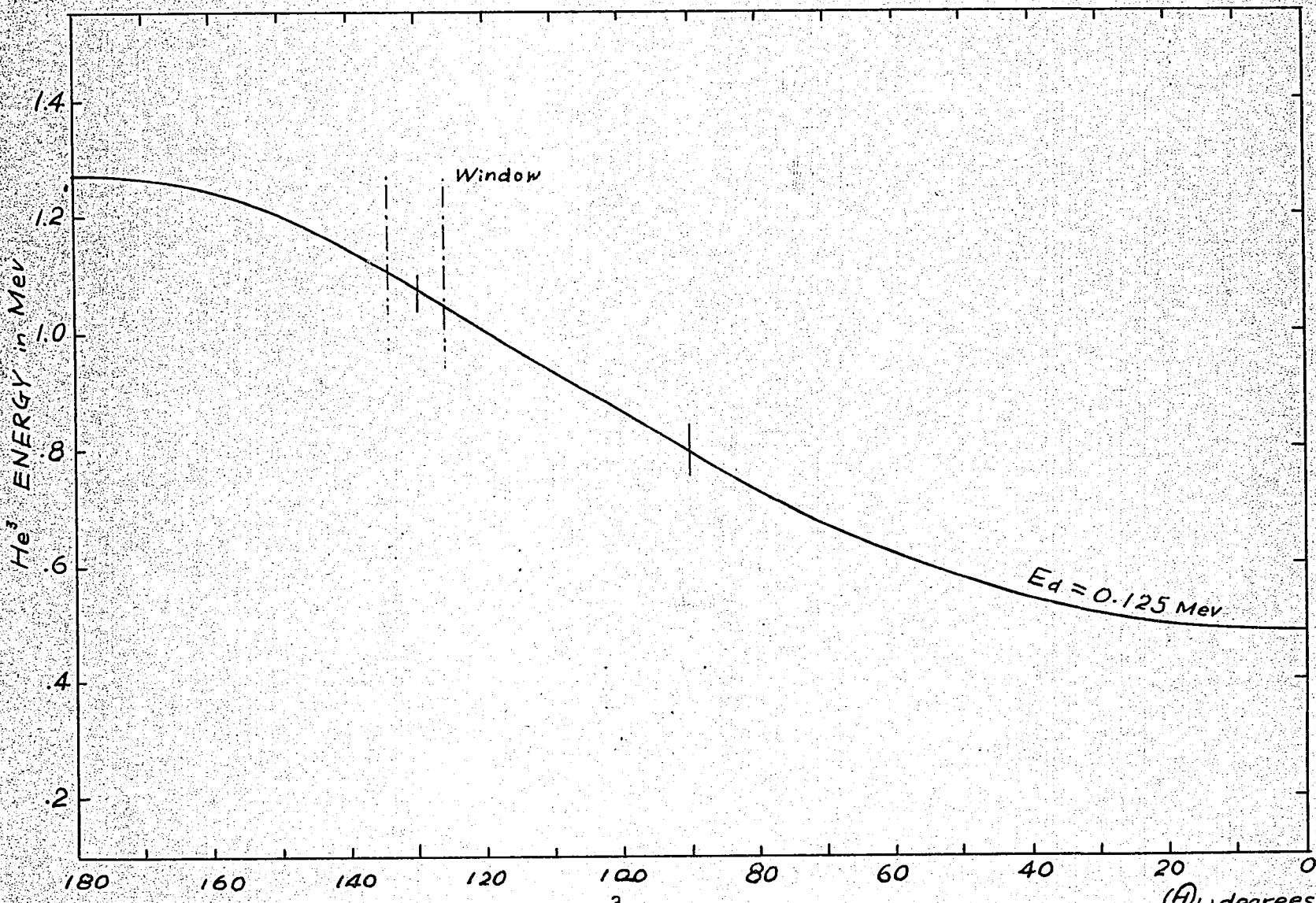

Fig. 19. The angle-energy dependence of the He^3 particles.

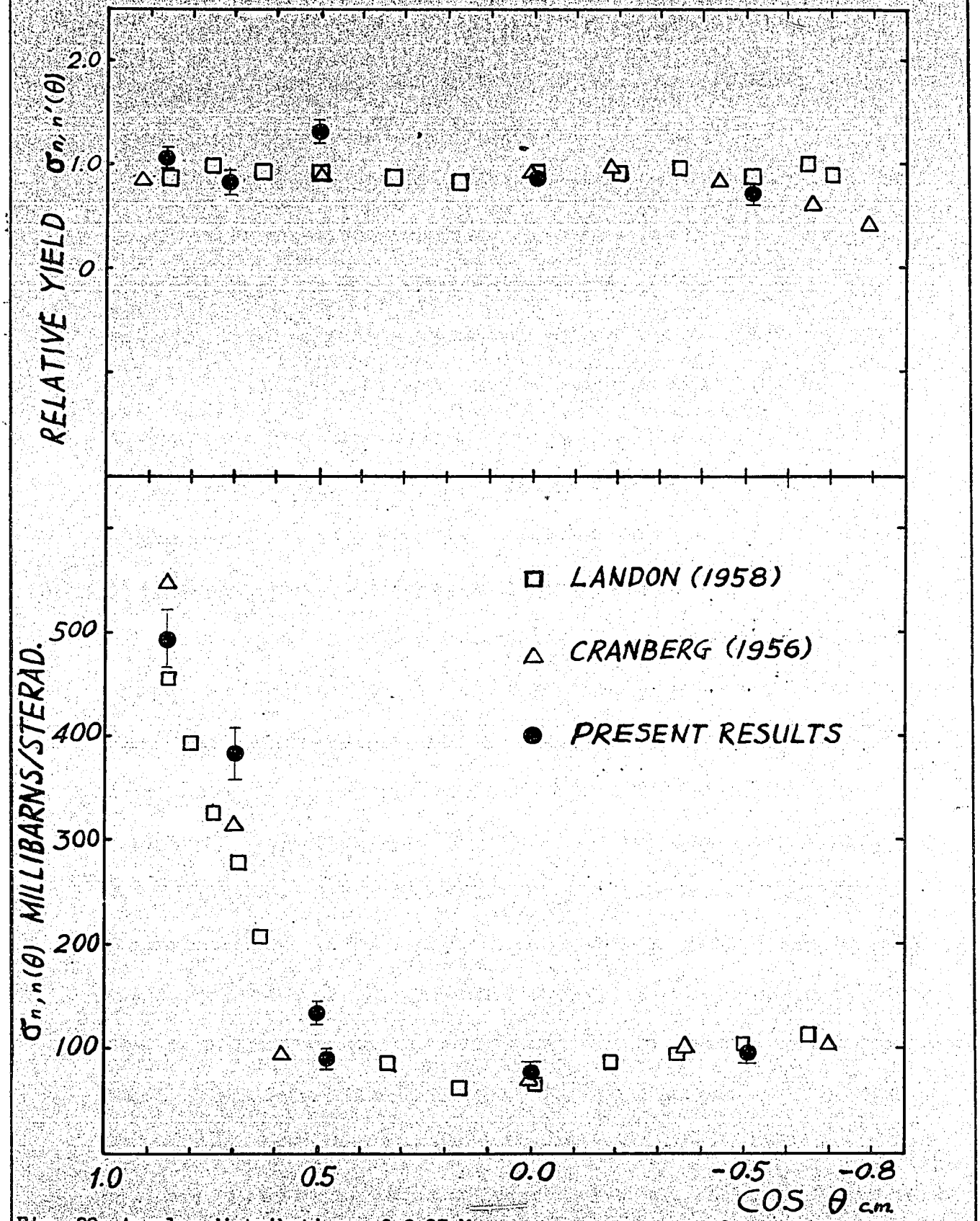

Fig. 20. Angular distributions of 2.37 Mev neutrons scattered from natural iron. (a) inelastic scattering from 0.845 Mev state. (b) elastic scattering.

without the scatterer on the scatterer holder, thus eliminating the serious uncertainties in the background.

The absolute values of the elastic cross sections were fixed by reference to the well-known n, p cross section[44]. This was measured at 45° using a polyethylene sample, $(-CH_2-CH_2-)_n$. The hydrogen content of the polyethylene had been estimated as 14.4% by weight.

Even with the same target and bombarding particles, there are two basically different types of reactions which can occur, depending on the size of the target nuclei, wave length of the incident projectiles and their properties. The different types of reactions are: (i) direct reaction, and (ii) compound reaction.

When an incident nucleon enters a target nucleus, it may simply be deflected by the nuclear potential and emerge again. Sometimes this incident nucleon may hit a nucleon and transfer some or all of its energy to one of the target nucleons. If the energy of either of these nucleons (projectile or target), exceeds its separation energy, then it may leave the nucleus without further interaction. This is a direct reaction. On the other hand, if none of the nucleons have exceeded their separation energy, they will continue to stay in the nucleus. Each nucleon will undergo further collisions. This is the formation of compound state. Since there are only few nucleons in the nucleus, after a period of collisions, sufficient amount of energy may concentrate on one of the nucleons, so that it may emerge from the nucleus. This is the compound

reaction.

The most significant features for these two types of reaction are their differential angular distributions. It is strongly forward peaked for the direct reaction. On the other hand it shows isotropic distribution for the compound reaction.

There have been successful explanations of the fast neutron elastic scatterings, by introducing the optical potential (with real and imaginary part), especially for neutrons at higher energy region. As the energy rises, a nucleon entering the nucleus may initiate a reaction. The nucleus can be thought of as a cloudy crystal ball, as first introduced by Feshbach et al. Some fraction of the incident neutron wave may be absorbed by the cloudy nucleus (imaginary part of the potential) and then may be re-emitted with a changed wavelength.

The present results for the elastic scattering are in agreement with those obtained by previous authors, thus justifying the use of the associated particle method for D-D neutrons. It would seem from the results that one could probably predict a good optical model fitting at incident energy of 2.37 MeV for iron.

On the other hand, the inelastic scattering from 0.845 MeV state shows an isotropic distribution. It appears from this that the compound nucleus model may be an adequate model for this case. Therefore it can be concluded that there are small contributions from the direct reaction at this energy.

CHAPTER 4

APPENDIX

4-1 dE/dx of He^3 at 0.785 MeV and 1.018 MeV in Aluminum.

The angular dependence of the energies of He^3 particles emitted from the D(d, n)He^3 was calculated from the formula:

$$\sqrt{E_{He^3}} = \frac{\sqrt{M_d M_{He^3} E_d}}{M_n + M_{He^3}} \cos\Theta \pm \sqrt{\frac{M_d M_{He^3} E_d}{(M_n + M_{He^3})^2} \cos^2\Theta + \frac{M_n}{M_n + M_{He^3}} \left\{ Q + E_d \left(1 - \frac{M_d}{M_n} \right) \right\}}.$$

where E_d, E_{He^3} are respectively the kinetic energies of the incident deuterons and outgoing He^3 particles. M_d, M_{He^3}, and M_n are the deuteron, He^3 and neutron masses. Q is the reaction energy and Θ is the angle of the outgoing He^3 particles in the laboratory system. Fig. 19 was plotted for E_d=0.125 MeV. This curve shows clearly that energetic He^3 particles can be detected at a still convenient angle of about 130°.

From Bethe's nonrelativistic dE/dx formula for heavy particles[45], and using the average excitation potential of aluminum as 150 ev[46], it was estimated that the He^3 particles emitted at the angle 130° with an energy of 1.065 MeV and at the angle 90° with an energy of 0.781 MeV have stopping powers of 3.82×10^3 MeV/cm and 3.54×10^3 MeV/cm respectively in the aluminum. Therefore after

passing through two layers of 150 $\mu g/cm^2$ aluminum foils, the remaining energies of He^3 particles from 130° and 90° are 0.672 MeV and 0.357 MeV respectively. The much higher residual energy of the He^3 at 130° led to the choice of this detection angle and made the associated particle method possible in the present work.

4-2 A Preliminary Measurement of Scattering from Al^{27}

A single measurement for the neutron scattering from aluminum at 90° was carried out. It took 30 hours to accumulate the spectrum as shown in Fig. 21. Although some data concerning Al scattering exist at the present time[47], it is felt that more precise studies for this particular nucleus are needed.

It is suggested that a useful continuation of this work will be to measure the differential cross sections and the angular distributions of the neutrons scattered from the 1.464 MeV level of argon 40. Because the melting point of argon is higher than the boiling point of liquid nitrogen it is possible to solidify argon by simply introducing a liquid nitrogen cooling system. A solid target could therefore be used for this proposed experiment. Nitrogen has a very low cross-section for both elastic and inelastic scattering[9]; especially at a neutron energy of 2.5 MeV the scattering from the first level of 2.31 MeV would be negligible. Therefore if one can construct the argon target container from a thin material, such as vinyl or steel, the serious background from target container can be avoided. Not only is no data available for the scattering from argon 40 presently, but also the spin of the first level is still undetermined. It would be possible to predict this spin by measuring the angular distribution using the theory of Hauser and Feshbach[48].

It would also be interesting to measure the scattering of neutrons from a liquid Ne^{20} target by using a special target assembly, because of the high natural abundance of Ne^{20}.

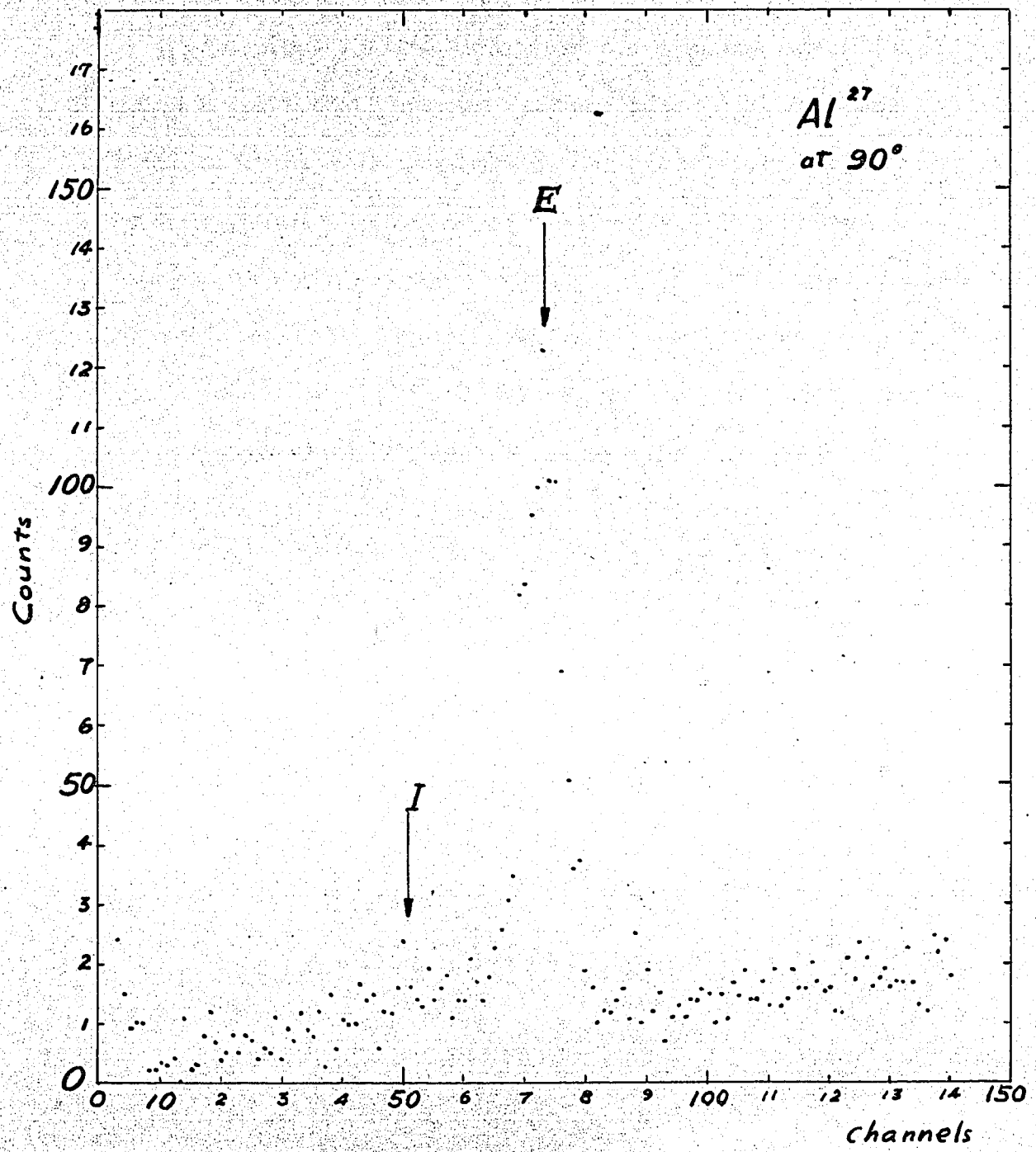

Fig. 21. The time-of-flight spectrum of the 2.37 Mev neutron scattering from aluminúm at 90°.

4-3 Illustrations

Plate 2 shows the neutron detector assembly. Plate 3 shows the used water tank and parrafin bricks neutron detector shielding. Sample electronics layouts are shown in Plates 4 and 5. Since the time-of-flight system requires ultra-fast pulses, great care had been paid for construction of all electronics components. Plate 4 is one of the neutron detector preamplifier which contains a fast limiter and a slow channel emitter follower. Plate 5 is the top-view of the fast discriminators and triple coincidence unit of Fig. 13.

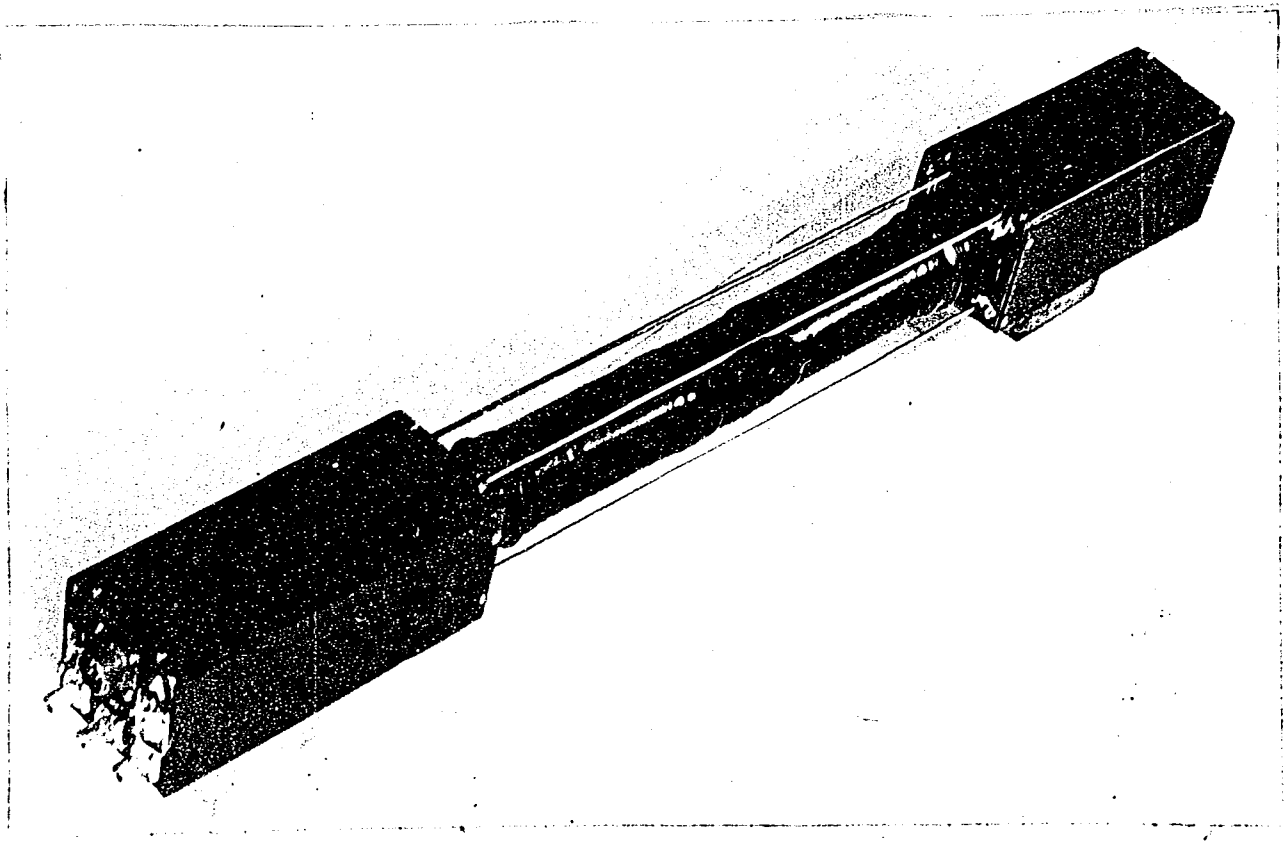

Plate 2 Neutron Detector Mounting

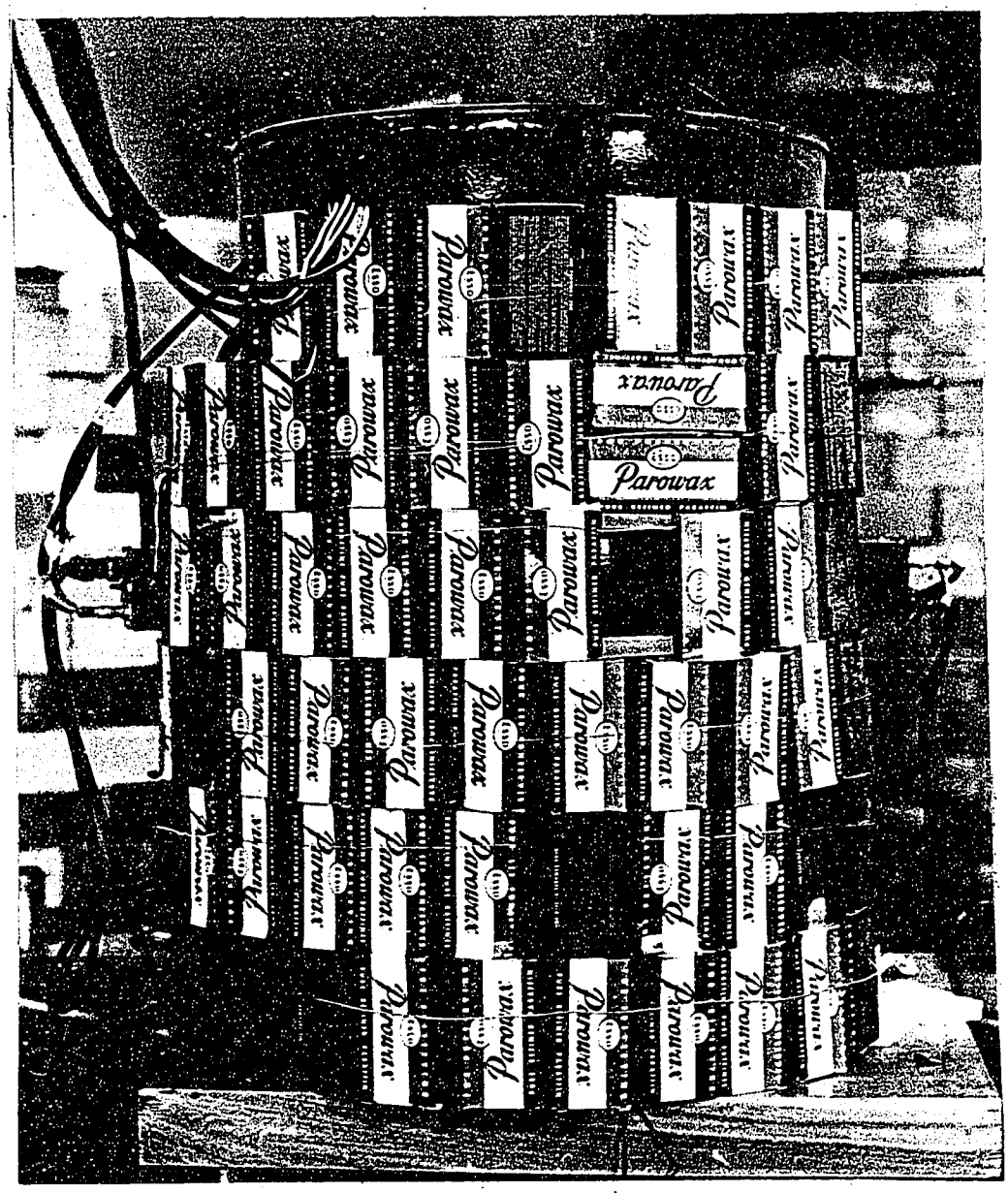

Plate 3 Neutron Detector Shielding

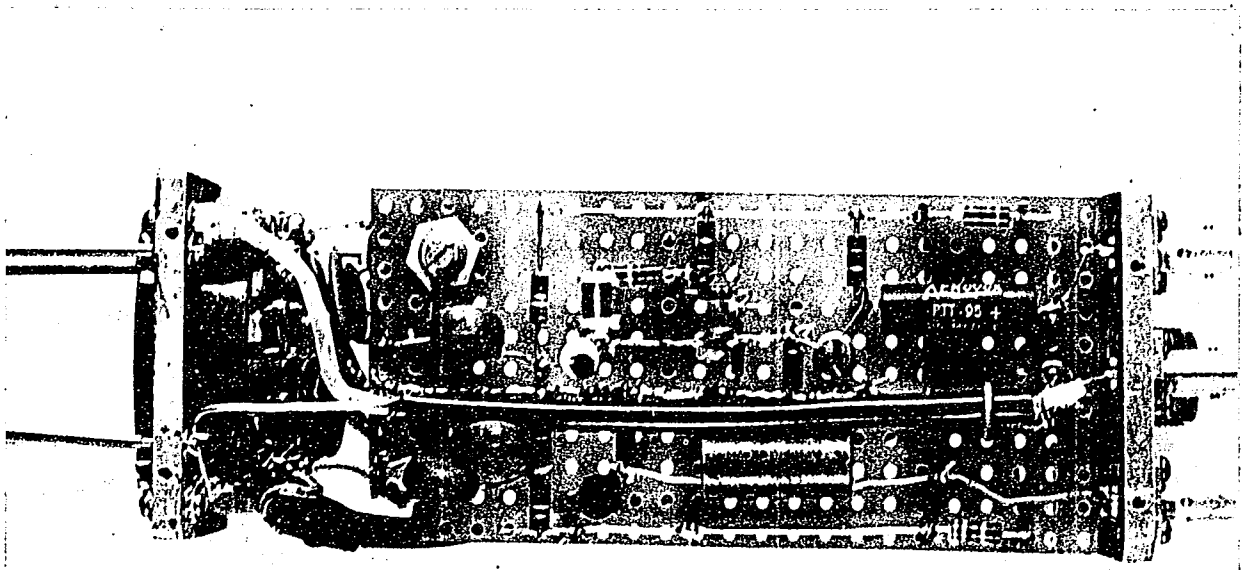

Plate 4 Neutron Detector Preamplifier (A)

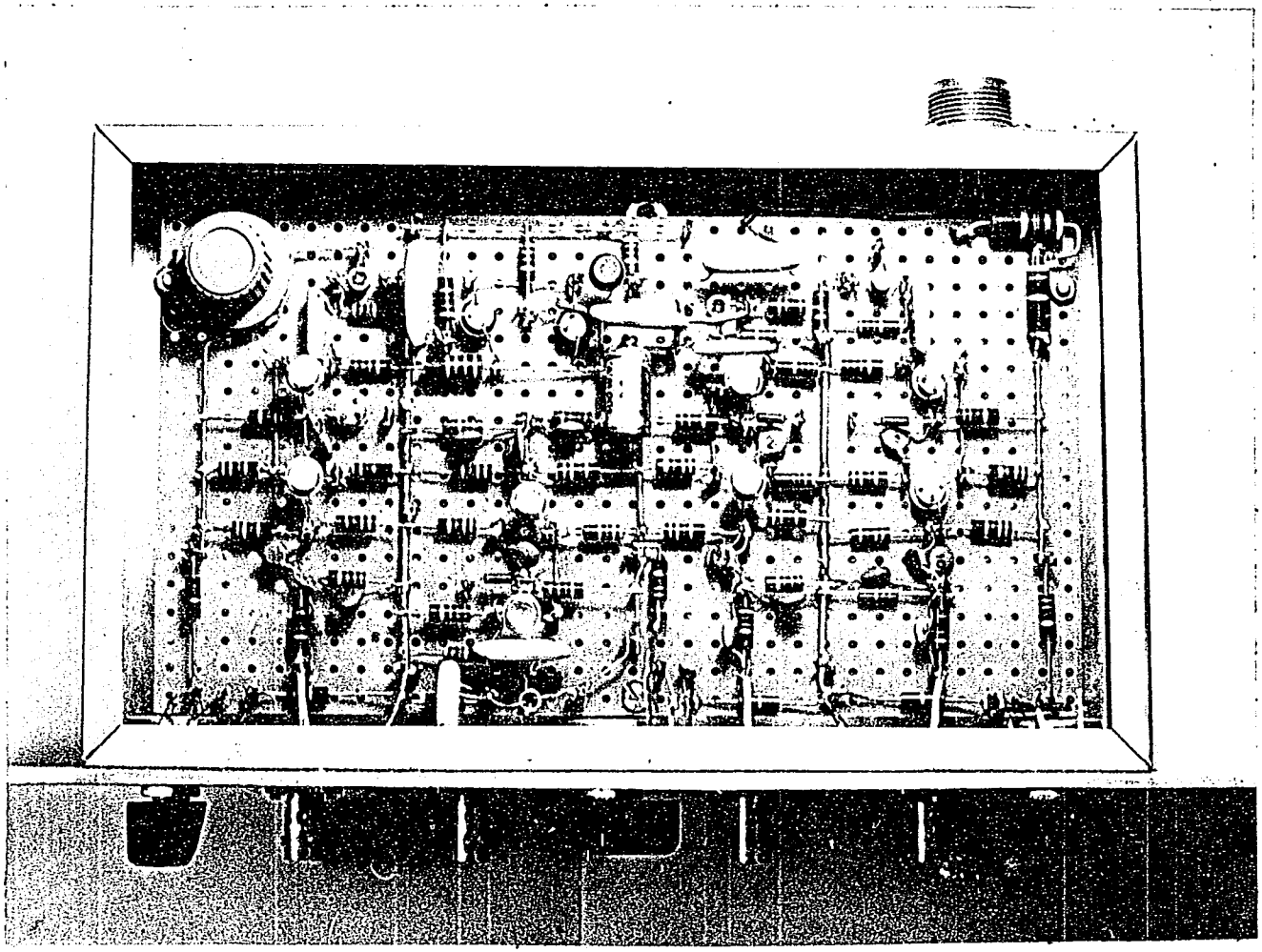

Plate 5 Fast Discriminators and Triple Coincidence

REFERENCES

1) L. Rosen and L. Stewart, Phys. Rev. 107, (1957), 824.

2) E. R. Graves and L. Rosen, Phys. Rev. 89, (1953), 343.

3) J.P. Conner, Phys. Rev. 89, (1953), 712.

4) J.D. Anderson, C. C. Gardner, M.P. Nakada and C. Wong, Phys. Rev. 110, (1958), 160.

5) C. St. Pierre, M.K. Machwe and P. Lorrain, Phys. Rev. 115, (1959), 999.

6) J. Rethmeier J., C.C. Jonker, M. Rodenburg, J. Hovenier and D. van der Meulen, Nuclear Phys. 38, (1962), 322.

7) Bobys et al., Soviet Phys. JETP 14, (1962), 18.

8) Strizhak, Soviet Phys. JETP 14, (1962), 225.

9) R. W. Bauer, J.D. Anderson and L. J. Christensen, Nuclear Phys. 47, (1963), 241.

10) R. N. Little J., B.D. Leonard, J., J. T. Prud'homme, and L.D. Vincent, Phys. Rev. 98, (1955), 634.

11) L. Cranberg and J.S. Levin, Phys. Rev. 103, (1956), 343.

12) J.R. Beyster, M. Watt, and E. W. Selmi, Phys. Rev. 104, (1956), 1319.

13) H.H. Landon, Phys. Rev. 112, (1958), 1192.

14) N. Nath, Nuclear Phys. 14, (1959), 78.

15) J. T. Prud'homme, P.L. Okuysen, and I.L. Morgan, Phys. Rev. 118, (1960), 1059.

16) K. Tsukada, S. Tanaka, and M. Maruyama, J. Phys. Soci. Japan 16, (1961), 166.

17) D. J. Donahue, Phys. Rev. 128, (1962), 1251.

18) J.H. Towle, Nuclear Phys. 32, (1962), 610.

19) J.H. Towle, Nuclear Phys. 44,(1963), 256.

20) D. Reitmann, C.A. Engelbrecht and A.B. Smith, Nuclear Phys. 48, (1963), 593.

21) R.O. Lane, A.S. Langsdorf J., J.E. Monahan, and Elwyn, Ann. Phys. 12, (1961), 135.

22) D. Winterhalter, Nuclear Phys. 39 (1962), 535.

23) B. Jennings, J. Weddell, and I. Alexeff, Phys. Rev. 98, (1955) 582.

24) P. Shapiro, V.E. Scherrer, B.A. Allison and W.R. Faust, Phys. Rev. 95, (1954), 751.

25) J. Rethmeier, Nuclear Instr. and Method 17, (1962) 273.

26) J.M. Freeman, Prog. in Nuclear Physics Vol. 5, Pergamon Press, (1956), 38.

27) R.B. Owen, Nucleonics 17, (1959), 92. (No.9)

28) Litherland, Almquist, Batchelor, and Gove, Phys. Rev. Letters 2, (1959), 104.

29) J.H. Coon, Fast Neutron Physics Vol. I., Interscience Pub., New York, (1960), 677.

30) C. Coceva, Nuclear Instr. and Methods, 21, (1963), 93.

31) F.D. Brooks, Progress in Nuclear Phys. Vol. 5, Pergamon Press, (1956), 252.

32) F.D. Brooks, Nuclear Instr. and Methods 4, (1959), 151.

33) W. Daehnick and R. Sherr, Rev. Sci. Instr. 23, (1961), 666.

34) F.W.K. Firk, Fast Neutron Physics Vol. II, Interscience Pub. New York, (1963), 2237.

35) R.B. Owen, Nucleonics 16, (1958), 54. (No.6)

36) R. Batchelor, W.B. Gilboy, A.D. Purnell and J.H. Towle, Nuclear Instr. and Methods 8, (1960) 146.

37) Anderson, Hincks, Johnson, Ray, and Segar, Phys. Rev. 133, (1964), B 392.

38) M.L. Roush et al., Technical Report 367, Dept. of Physics and Astronomy, University of Maryland, March 1964.

39) R.E. Green and R.E. Bell, Nuclear Instr. and Methods 3, (1958) 127.

40) A. Langsdorf, Fast Neutron Physics Vol. I, Interscience Pub., New York, (1963) 721.

41) B.V. Rybakov and Sidrov, Fast Neutron Spectroscopy, Consultants Bureau, Inc., New York, (1960).

42) J.H. Neiler and W.M. Good, Fast Neutron Physics, Vol. I., Interscience Pub., New York (1960), 509.

43) L.I. Schiff, Quantum Mechanics, McGraw-Hill, (1955), 97.

44) Hughes, Brookhaven, National Report, BNL 325, (1958).

45) E. Segre, Experimental Nuclear Physics Vol. I, (1953), 167.

46) R.R. Wilson, Phys. Rev. 60 (1941) 749.

47) D. Winterhalter, Nuclear Phys. 43, (1962), 339.

48) W. Hauser and H. Feshbach, Phys. Rev. 87, (1952), 366.